Spring 2009

Investment shell cracking

Edward A. Druschitz

Department:

INVESTMENT SHELL CRACKING

by

EDWARD ALAN DRUSCHITZ

A THESIS

Presented to the Faculty of the Graduate School of the

MISSOURI UNIVERSITY OF SCIENCE AND TECHNOLOGY

In Partial Fulfillment of the Requirements for the Degree

MASTER OF SCIENCE IN MATERIALS ENGINEERING

2009

Approved by:

Dr. Von L. Richards, Advisor
Dr. Ronald Kohser
Dr. Frank Liou

PUBLICATION THESIS OPTION

This dissertation consists of three articles submitted for publication as follows. Each article is prepared according to the respective style of the publication. Pages 3-17 have been submitted for publication in the International Journal of Cast Materials. Pages 18-32 have been published by The Minerals, Metals, and Materials Society. Pages 33-45 have been published by the Investment Cast Institute.

ABSTRACT

Shell cracking is the single greatest problem affecting investment casters. A clearer understanding of the factors affecting the melt profile of the wax can be gained using computational fluid dynamics (CFD) to model the interaction among 1) the thermal conductivity of the wax, 2) the thermal conductivity of the shell, and 3) the temperature of the autoclave during the autoclave de-waxing cycle. The most favorable melt profile results from a high autoclave temperature (438°K to 458°K) and saturated thermal conductivity of the shell (1.36 to 1.40 $Wm^{-1}k^{-1}$) in conjunction with a low wax thermal conductivity (0.33 $Wm^{-1}k^{-1}$). These parameters reduce the likelihood of shell cracking as a result of wax bulk expansion.

Thin wall ice patterns can be invested by coating patterns with a tridecane interface agent, using a 20 wt% ethyl silicate binder with 20 wt% fiber-containing fused silica flour added after the primary coat, delaying the application of the catalyst by 4 hours, and maintaining a -10°C environment. A -10°C or lower environment increased shell strength and improved surface finish. It also found that tridecane resulted in a 7% loss of thickness in ice 3.175mm (0.125 inches) and thicker.

Oxidation along the leading edge of cast Fe-15Cr-4.5Ni-3Cu (15-5 PH) stainless steel marine propellers leads to costly non-value added finishing. The addition of an extra seal coat of slurry after autoclaving and a slower cooling rate can reduce oxidation by 1.7 to 1.4mm^2mm^{-1} of oxidation per millimeter of blade length.

ACKNOWLEDGMENTS

First and foremost, I would like to thank Dr. Von Richards; without him none of this would have been possible. He has been more patient then I could ever have hoped as I have stumbled to gain a foothold in metallurgy. His time and patience have been greatly appreciated during my struggle to understand materials engineering.

Next, I would like to thank my committee members, Professor Ronald Kohser and Professor Frank Liou for their guidance and time. They have helped me gain a fundamental understanding of key issues important to this research.

I would also like to thank my family, Alan, Lori, and Laurel. Without my father's constant guidance, patience, and undying support I may not have seen this through to the end; he is a constant inspiration for me. He is my role model as a developing professional in the metallurgical field. My mother and sister have been constant pillars of support, and I cannot thank them enough.

In addition, I would like to thank a few professors who have also helped me greatly during my time here: David Van Aken, Greg Hilmas, Jeffrey Smith, William Fahrenholtz, and Mary Reidmeyer, your constant words of encouragement have helped me more then any of you know.

I would also like to thank a few graduate students who have helped me stay on track and at times reminded me to never give up: Hank Rawlins, Ryan Howell, and William Dewy Peach, you have truly helped me find myself as a graduate student and a person.

TABLE OF CONTENTS

LIST OF ILLUSTRATIONS

LIST OF TABLES

1. INTRODUCTION

Investment casting can be considered either a new or an old technology, depending on one's perspective on industrial history and genealogy. Industrial investment casting began with the need for intricate turbine blades during World War II. However, the process of lost wax dates back to pre-Christian Egypt and Chinese dynasties as early as 4,000 BC. Older pots, vases, wine goblets, and religious artifacts display intricacy achieved using lost wax. Older methods of investing the wax involved packing clay around bee's wax patterns before firing, creating castings devoid of parting lines. However, advances in ceramics and shell building dramatically changed the investment casting industry. Corning Glass Works patented and marketed a technique called Glascast in 1957; simultaneously, Watertown Arsenal introduced a process called sintered alumina mold. Both processes are recognized as the original ceramic shell, nonflask, investment casting technique [AFS, 1993]. Investment casting begins with the creation of a wax part by injection. The part is assembled into a tree wherein numerous parts share a single downsprue. The tree is invested and stuccoed before removing the wax using an autoclave or boilerclave. The shell is fired to add strength before filling with molten metal. The metal is allowed to cool before removing the castings for finishing.

The primary goal of this research was to reduce or eliminate shell cracking in investment castings. This project involved: 1) continuing efforts to develop a predictive parametric model of autoclave dewaxing, since cracking often occurs in the autoclave process, 2) building thin wall shells for the casting of aluminum metal matrix composites using ice patterns in association with rapid freeze prototyping (RFP) technology, and 3)

reducing cracking during solidification after pouring, resulting in increased casting quality in cast 15-5 PH marine propellers.

Parametric studies on heat flow and melt front progression should be conducted to determine real world boundary conditions via computer modeling of autoclave temperature, shell thermal conductivity, and wax conductivity.

Many problems arise from the volumetric expansion of wax during the autoclave de-waxing cycle. Extensive research has sought to alleviate or eliminate these issues; however, most remain unresolved. As a result, RFP and freeze casting have a bright future. However, numerous avenues of research remain open: Parameters must be developed for building thin wall shells, and interface agents are needed to limit binder/water interactions. In addition, shell strength and casting surface finishes could be improved. Finally, pattern loss must be addressed.

To reduce premature cracking during cooling (post pouring) at Mercury Marine, ceramic strengthening techniques and binder systems (e.g. colloidal silica) were modified to increase shell toughness. Four-point bend test bars enabled quantitative comparison of changes made to the shell mold system. Quantitative image analysis allowed for the comparison of oxidation amounts normalized by blade length.

I. Parametric Modeling of the Autoclave De-waxing Process

Edward A. Druschitz

Missouri University of Science and Technology, Rolla, Missouri

Keywords: Investment Casting, Autoclave, Shell Cracking

1. ABSTRACT

Snow [1998] suggested that up to 90% of all shell cracking is a result of the autoclave dewaxing cycle. The majority of cracks are caused by bulk expansion of the wax as it is heated. The expanding wax stresses the shell, and if the stress intensity becomes greater than the shell's strength, the shell cracks. Minimizing the expansion of the wax during melting eliminates these cracks. A clearer understanding of the factors affecting the melt profile of the wax can be gained by using computational fluid dynamics (CFD) to model the interaction among 1) the thermal conductivity of the wax, 2) the thermal conductivity of the shell, and 3) the temperature of the autoclave. The most favorable melt profile results from a high autoclave temperature (438°K to 458°K) and saturated thermal conductivity of the shell (1.36 to 1.40 $Wm^{-1}k^{-1}$) in conjunction with a low wax thermal conductivity (0.33 $Wm^{-1}k^{-1}$). These parameters reduce the likelihood of shell cracking as a result of wax bulk expansion.

2. INTRODUCTION

Investment casting foundries use a saturated steam autoclave to remove wax patterns from ceramic shells made of fused silica. Cracks nucleated by the autoclave may result in leakers (run-outs), dimensional distortion, surface defects, and inclusions. The majority of these cracks are caused by the bulk expansion of the wax during melting. Minimization of this expansion would drastically reduce shell cracking and associated defects. Figure 2.1 illustrates the autoclave de-waxing cycle.

The autoclave process occurs in the following steps:

1. The shells are placed inside the autoclave.
2. Water is flash boiled into steam and injected into the autoclave.
3. Steam condenses on surfaces of sub-superheated steam temperatures.
4. Water permeates the shells (increasing thermal conductivity).
5. Wax begins to melt at the shell/wax interface causing a volumetric expansion.

Cracking is a nucleation and growth process. Cracks form in the autoclave when stresses caused by the bulk expansion of the wax exceed the strength of the shell. Cracks grow along the path of least resistance in order to alleviate the stress caused by bulk expansion. Stresses can be relieved by the lateral flow of liquefied wax through vents and gating.

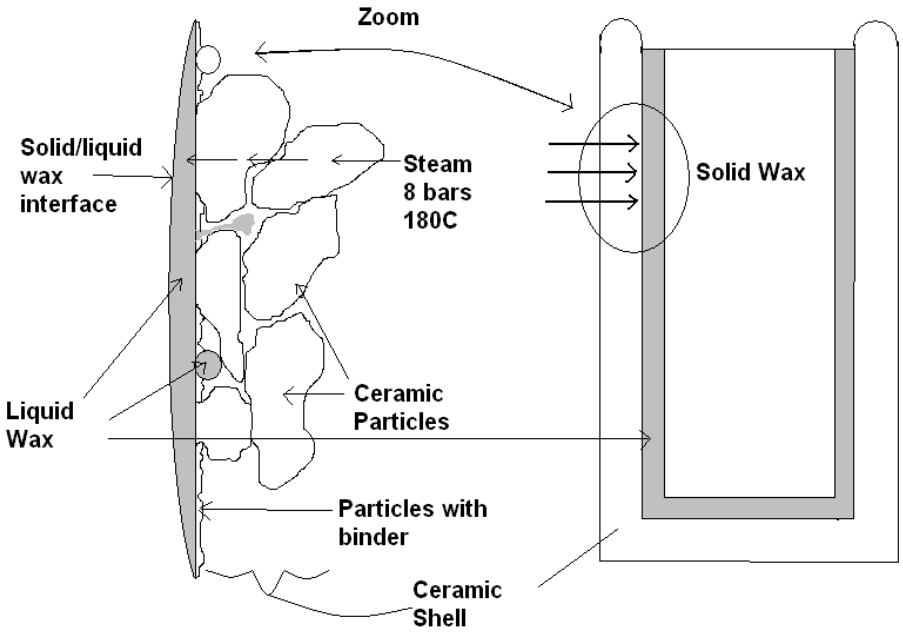

Figure 2.1. Schematic of heat transfer in the autoclave. Steam condenses on the shell's surface and saturates the shell. Heat is transferred through the shell to the under lying wax, resulting in melting [Gebelin, 2001].

Snow [1998] estimated that a dry fused silica shell has a thermal conductivity of 2.00 X 10^{-5} BTUsec^{-1}in°F (1.5 Wm^{-1}K^{-1}). He also estimated that a shell with 25% porosity filled with water would have a conductivity of 4.21 X 10^{-5} BTUsec^{-1}in°F (3.15 Wm^{-1}K^{-1}). Kruse and Richards [2005B] measured the dry shell's thermal conductivity at 0.5 Wm^{-1}K^{-1} and the saturated shell's thermal conductivity at 1.4Wm^{-1}K^{-1}.

Once the shell surface is saturated with water, the pressure inside the autoclave puts the shell in a compressive state of stress until the wax expands volumetrically. Fused silica undergoes negligible expansion as it is heated from room temperature to the autoclave operating temperature.

In early instrumented autoclave trials, Jones et al. [2001] found that the interior of an autoclave reaches its maximum temperature and pressure in less than ten seconds.

Later work conducted by Kruse and Richards [2005A] showed that within forty seconds the outer surface of the shell reached ambient autoclave temperature. In either case, during the de-waxing process the environmental temperature boundary condition occurs quickly at the surface of the shell. This is considered in modeling in that, the rapid development of this condition allows the modeler to ignore the remainder of the autoclave and apply a constant temperature boundary condition at the shell surface when constructing the model.

Mathematical models for estimating the thermal conductivity of ceramic-water porous phase composite structures include: Maxwell, Sson–Frey, Russel, and Bruggeman [Kruse and Richards 2005B]. These methods result in a dry shell thermal conductivity range of 0.05 to 0.20 $Wm^{-1}K^{-1}$ and a water saturated thermal conductivity range of 0.20 to 0.80 $Wm^{-1}K^{-1}$ [Kruse and Richards, 2005B]. Kruse and Richards [2005B] determined that dry and water saturated shell thermal conductivities are 0.5 and 1.4 $Wm^{-1}K^{-1}$, respectively. They interpreted the discrepancy between modeled conductivity and measured results stemmed from the inability of previous models to account for a combination of continuous and non-continuous phases within the shell. Snow [1998] assumed condensed water from the steam was pulled into the shell via capillary action due to high pressures. Kruse [2005] and Kruse and Richards [2005B] proposed a modified Maxwell model that accounted for the change in the thermal conductivity of a continuous phase as a function of temperature. This model best fit the experimentally measured data.

These data were used to generate a parametric model to determine the heat flow through the shell and melt front progression through the wax. The wax pattern's thermal

absorption consists of a sensible heat increase, $C_p\Delta T$, and a latent heat of fusion during melting, $m_{liq}\Delta H_f$ [Kruse and Richards, 2005B].

The main focus of the work presented here is the development of a parametric thermal model to evaluate for the influence of 1) pattern wax thermal conductivity, 2) investment shell thermal conductivity, and 3) autoclave temperature on melt front progression and its resulting effects on the bulk expansion of the wax.

3. BOUNDARY CONDITIONS AND PARAMETERS

A rectangular block of wax (10 mm×100 mm×100 mm) was chosen for the current study to allow for an infinite plate approximation and to reduce the edge effects. The shell was set at 12 mm thick (the average of shells from three industrial sources). The shell surrounded the entire wax block, as shown in Figure 3.1. Heat transferred through the shell to the underlying wax resulted in melting and a thermal gradient through the wax.

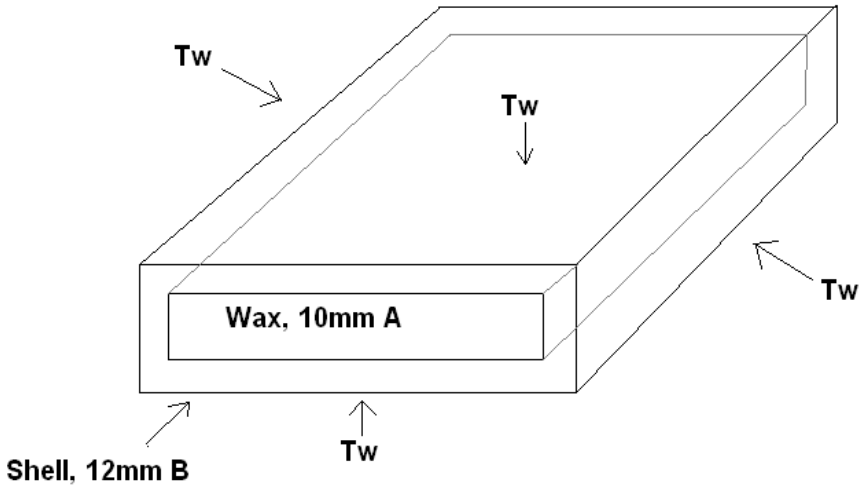

Figure 3.1. Wax block surrounded by ceramic investment casting shell with boundary condition T_w (temperature at wall).

The thermal resistance between the materials at their boundaries was ignored because the thermal conductivity of the shell material is low. Fluid flow was also ignored for the purpose of this parametric model. A semi-infinite plate solution boundary condition allowed the edge effects to be ignored. This permitted simplification of a three dimensional computer model to a two dimensional simulation.

For this parametric model, the fixed boundary condition was a constant shell surface temperature (T_w) set at values of 433^{o}K, 438^{o}K, and 458^{o}K (T_w) as per the results of Jones et al. [2004] work on the thermal profiles of autoclaves. Table 3.1 lists the conditions and variables used for ten simulation runs. The three variables in these tests were: a) wax thermal conductivity, b) shell thermal conductivity, and c) autoclave (shell surface) temperature.

Table 3.1. Parameters used to determine the influence of shell and wax conductivity and autoclave temperature on the melt profiles of wax during autoclaving.

Name	Shell Thermal Conductivity ($Wm^{-1}K^{-1}$)	Wax Thermal Conductivity ($Wm^{-1}K^{-1}$)	Autoclave Temperature (°K)
Model 1	0.55	0.33	438
Model 2	0.55	0.5	438
Model 3	1.36	0.33	438
Model 4	1.36	0.5	438
Model 5	1.4	0.33	438
Model 6	1.4	0.5	438
Model 7	1.36	0.33	433
Model 8	1.36	0.5	433
Model 9	1.36	0.33	458
Model 10	1.36	0.5	458

The shell's thermal conductivity was varied between three different values: 0.55, 1.36, and 1.4 $Wm^{-1}K^{-1}$, representing a "dry" (model one and two) and a fully water saturated shell respectively. The last two values (1.36 and 1.4) were chosen to determine the sensitivity of the modeled system to small changes in wax thermal conductivity. The typical autoclave cycle is 30 to 40 minutes. Backup coats saturate 15 seconds after the door is closed. The primary coat saturates in 80 seconds. Therefore, saturated shell conductivity was used in the remaining simulations. Wax thermal conductivity was varied between 0.33 $Wm^{-1}K^{-1}$ (for low density polyvinyl ether polymer) and 0.5 $Wm^{-1}K^{-1}$ (for high density polyvinyl ether polymer). Additional properties required for the simulation are summarized in Table 3.2; the additional properties of the low density polyvinyl wax were held constant regardless of thermal conductivity to eliminate their impact on the results.

Table 3.2. Additional properties of the wax and shell required for the completion of the parametric simulation.

	Density	Cp	Hf	Solidus	Liquidus
Material	(Kgm-3)	(JKg-1K-1)	(JKg-1)	(K)	(K)
Polyvinyl Wax	1350	1250	300000	339	349
Shell	2201	703			

A quadrilateral face with a three-node edge and both tetrahedral and cubic volumes was used to mesh the shell and wax respectively. All calculations were conducted assuming an unsteady state with segregated calculations. Each time step was recorded in Fluent at 2.0 seconds, with a computational time step of 0.01 seconds. At each time step, the thickness of the melt front was calculated and saved in an Excel spreadsheet. Complete melting was defined as a liquid fraction greater than 85%. Figure 3.2 is an example of the 2D slice generated by Fluent software and used to predict the thickness of the wax melt front. In this figure, blue indicates solid material and red indicates melted material. Melt front thickness was determined by measuring the thickness of the red area at a cross-section of the plate's center. Heat was transferred through the shell to the underlying wax, causing it to melt. This transfer resulted in a thermal gradient due to low thermal conductivity of the wax.

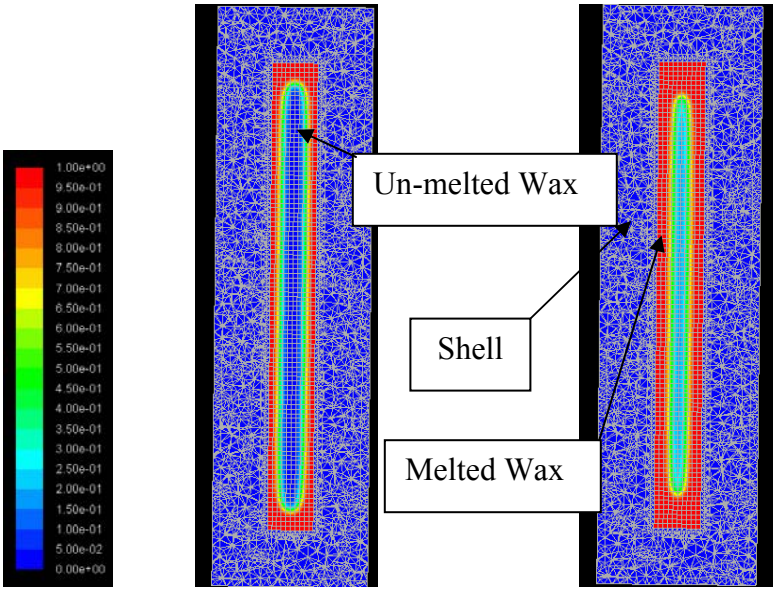

Figure 3.2. Melt profiles of the wax as a result of the calculated distribution of the liquid fraction at 480s (left) and 640s (right).

4. COMPUTATIONAL PROCEDURES

The enthalpy-porosity technique was used to model the phase change process. The melt interface was not tracked explicitly; instead, the liquid fraction associated with each control volume in the domain and computed each iteration. The liquid fraction, therefore, varied between zero (solid) and one (liquid). The energy equation is written in terms of sensible enthalpy, h, defined as equation 1

$$h = h_{ref} + \int_{T_{ref}}^{T} c_p dT \tag{1}$$

where h_{ref} in J is the reference enthalpy, T_{ref} in K is the reference temperature, and c_p is specific heat at constant pressure in $Jkg^{-1}K^{-1}$, and is a function of temperature T. The enthalpy can be computed as the sum of the sensible enthalpy h and the latent heat ΔH (equation 2)

$$H = h + \Delta H \tag{2}$$

In addition, the latent heat content (ΔH) may vary between zero (solid) and L (liquid), the latent heat of the material. As a result, the liquid fraction (β) can be defined as equation 3 if $T_{Solidus} \leq T \leq T_{Liqudus}$.

$$\beta = \frac{\Delta H}{L} = \frac{T - T_{solidus}}{T_{liquidus} - _{solidus}} \tag{3}$$

For phase change problems, the energy equation is written as equation 4

$$\frac{\partial}{\partial t}(\rho h) + \frac{\partial}{\partial t}(\rho \Delta H) + \frac{\partial}{\partial x_i}(\rho u_i h) = \frac{\partial}{\partial x_i}(k \nabla T) + S \tag{4}$$

where H, h, and ΔH in (J) is the enthalpy of the wax, ρ (kgm^{-3}) is the density of the wax, k (Wm^{-1}K^{-1}) is the thermal conductivity, T (K) is the temperature, and S is the source term, t is the time in seconds, u_i is the fluid velocity in ms^{-1}, and x_i is Cartesian coordinate directions. Fluid flow is irrelevant, thus the velocity term $\frac{\partial}{\partial x_i}(\rho u_i h)$ is reduced to zero. Using Equation 3, the sensible enthalpy (h) and the latent heat content (ΔH) equal the enthalpy (H). As such, equation 4 can be reduced to Equation 5.

$$\frac{\partial}{\partial t}(\rho H) = \frac{\partial}{\partial x_i}(k \nabla T) \tag{5}$$

This leaves five unknown variables: H, T, h, ΔH, β and five equations (Eq.1-3 and 5).

5. RESULTS

Reporting the results requires the definition of several critical times:

T_{ms}: the time required for melting to begin on the outer surface of the wax.

T_{mo}: the time required for melting to finish on the outer surface.

T_{mc}: the time required for melting to begin in the center of the wax.

T_{mi}: the time required for melting to finish half way to the center.

T_{mf}: the time required for melting to finish at the center of the sample.

DT: the time difference between the completion of melting on the outer wax surface and the beginning of melting at the center.

The results of all simulations are shown in Table 5.1. Low conductivity shells resulted in negative DT times (-72 and -134). Saturated shell conductivity resulted in a positive DT time. Increased autoclave temperature, saturated shell conductivity, and low wax thermal conductivity resulted in the highest DT time of 48 seconds.

Table 5.1. Times required for melting given varying shell and wax conductivities and autoclave temperatures. Increased autoclave temperature, saturated shell conductivity, and low wax thermal conductivity resulted in the highest DT time of 48 seconds.

Model	Shell Thermal Conducivity (W/(m*K))	Wax Thermal Conducivity (W/(m*K))	Autoclave Temperature (K)	Elapsed Time to Event (sec)					
				Tms	Tmo	Tmc	Tmi	Tmf	DT
1	0.55	0.33	438	154	352	280	662	878	-72
2	0.55	0.5	438	156	374	240	648	802	-134
3	1.36	0.33	438	60	138	178	312	484	40
4	1.36	0.50	438	62	138	144	286	412	6
5	1.40	0.33	438	58	134	174	306	476	40
6	1.40	0.50	438	60	134	142	278	404	8
7	1.36	0.33	433	62	144	180	328	504	36
8	1.36	0.50	433	64	144	146	300	430	2
9	1.36	0.33	458	54	118	166	266	416	48
10	1.36	0.50	458	54	118	134	242	354	16

6. DISCUSSION

A high DT value will reduce the stress on the shell caused by the bulk expansion of the remaining wax. Therefore, the outer layer of the wax should ideally finish melting (T_{mo}) prior to significant temperature increase at the center of the pattern (T_{mc}).

The first set of simulations (model one and two) studied the effect of the waxes' thermal conductivity on melt times. When the thermal conductivity of the shells and the autoclave temperature were held constant at 0.55 $Wm^{-1}K^{-1}$ (dry) and 438°K respectively, the low conductivity of the shell limited the amount of heat transferred to the wax. In both cases, the wax began to melt at its center before it finished melting at its surface. The low thermal conductivity of the shell is unfavorable since it will lead to a large bulk expansion (indicated by a negative DT time).

Models three through six demonstrate that saturated shell conductivities lessen the effect of wax thermal conductivity on the time required for melting to begin and finish on the surface (T_{ms} and T_{mo}). However, the higher thermal conductivity wax (models four and six) began to melt in the center six seconds after it finished melting at the surface. The higher shell thermal conductivity in conjunction with lower conductivity wax (models three and five) result in a more favorable melt profile (larger DT), reducing the likelihood that the wax will undergo bulk expansion and result in shell cracking.

The last of the simulations (models seven through ten) determined the impact of autoclave temperature. Wax thermal conductivity did not affect the time required for initiation and completion of melting on the surface. The increased autoclave temperature and low conductivity wax resulted in the greatest DT time of 48 seconds.

7. CONCLUSIONS

Favorable profiles are defined as having the greatest possible time delay between completion of melting on the wax's surface and beginning of melting at the wax's center (DT). These profiles should limit the bulk expansion of the wax and thereby reduce the likelihood of shell cracking. Low thermal conductivity dry shells (0.55 $Wm^{-1}K^{-1}$) in conjunction with high wax conductivity (0.5 $Wm^{-1}K^{-1}$) produced the least favorable melting profiles (DT of -134 seconds). High autoclave temperatures (438-458°K), high conductivity saturated shells (1.36-1.40 $Wm^{-1}K^{-1}$), and low conductivity wax (0.33 $Wm^{-1}K^{-1}$) resulted in the most favorable melt profiles (DT of 48 seconds).

8. FUTURE WORK

Future work should include the addition of wax expansion data in order to calculate the stress applied to the shell. Data on the flow of fluid out of the shell should also be added to the simulation in order to calculate the alleviation of stress.

9. REFERENCES

American Foundrymen's Society. Handbook on the Investment Casting Process. Des Plaines, Illinois: American Foundrymen's Society, 1993.

Gebelin, J. & Jones, S. "Modeling of the De-Waxing of Investment Cast Shells". TMS 2001.

Jones, S. Jolly, M. Blackburn, S. Gebelin, J. Cendrowicz, A. and Lewis, K. "Measurements of autoclave thermal profiles during high pressure steam de-waxing of investment shells: Part 1 – Vessel profiles." Materials Science and Technology, May 2005. Vol. 20.

Jones, S. Jolly, M. Gebelin, A. Cendrowicz, A. & Lewis, K. "To Boldly Go Where No Woman Has Gone Before: Dewaxing Results From FOCAST." ICI 49th Annual Meeting, 2001.

Kruse, B. "Mold and Metal Interactions in Highly Alloyed Steels", M.S. thesis, University of Missouri-Rolla, 2005.

Kruse, B. & Richards, V. "Success of a Data Acquisition System Designed to Measure Thermal, Moisture and Pressure Profiles in Production Autoclaves". ICI 53rd Annual meeting, Paper #15, 2005.

Kruse, B. & Richards, V. "Thermal and Moisture Characterization During Autoclave Dewaxing in Investment Casting." SFSA T&O Conference, Paper # 5.5, 2005.

Snow, J. "What Happens During Autoclave Dewaxing". Investment Casting Institute 46th Annual Technical Meeting. 1998.

II. Investment Shell Building on Ice Patterns

Edward A. Druschitz

Missouri University of Science and Technology, Rolla, Missouri

Keywords: Investment Casting, Rapid Freeze Prototyping, Ice Casting

1. ABSTRACT

This work developed shell building techniques for rapid freeze prototyping (RFP). Thin wall ice patterns were invested by coating patterns with a tridecane interface agent, using a 20 wt% ethyl silicate binder with 20 wt% fiber-containing fused silica flour added after the primary coat, delaying the application of the catalyst by 4 hours, and maintaining a -10°C environment. Finished shells were quantitatively evaluated by determining mold cavity dimensional reproducibility and shell strength. Tridecane proved an effective interface agent and resulted in stronger surface coats. It was particularly beneficial when combined with greater pattern thermal mass, which delays melting for a longer period of time. A -10°C or lower environment increased shell strength and surface finish. Tridecane resulted in a 7% loss of thickness in ice 3.175mm (0.125 inches) and thicker.

2. INTRODUCTION

Water does not undergo volumetric expansion as it melts. Yodice [1991, 1998, 1999] first proposed water (ice) as a pattern material for investment casting. Rapid freeze prototyping is a solid freeform fabrication technique wherein water droplets form frozen layers of ice that generate thin-wall investment casting patterns. This method and material combination allows investment casters to produce prototype patterns rapidly, and it obviates the disadvantages of previous technologies.

Wax undergoes a volumetric expansion during melting, which can result in shell stresses great enough to cause shell cracking. Commercially available rapid prototyping polymers undergo a greater volumetric expansion than typical pattern waxes, increasing the likelihood of shell cracking.

Rapid prototyping, or solid freeform fabrication (SFF), is a commercialized method for quickly producing three-dimensional parts via layer-by-layer deposition. This technique allows manufacturers to produce prototype parts rapidly, while decreasing development time and reducing cost, and increasing quality. Typical rapid prototyping materials undergo greater volumetric expansion than standard pattern wax or demonstrate such poor fluidity compared to industrial pattern waxes that additional drain offs must be cut into the ceramic mold, adding man hours and reducing overall part quality.

Figure 2.1. is an image of RFP equipment; the XY table moves, allowing the nozzle to deposit water droplets on the liquid nitrogen chilled substrate. A freezer houses the entire unit; water is pumped to the nozzle via an external pump. Continuing development of this process for industrial use focused on taking thin-walled ice patterns, building investment shells on them, determining ice pattern thickness reproducibility and producing metal-matrix-composite (MMC) aluminum castings.

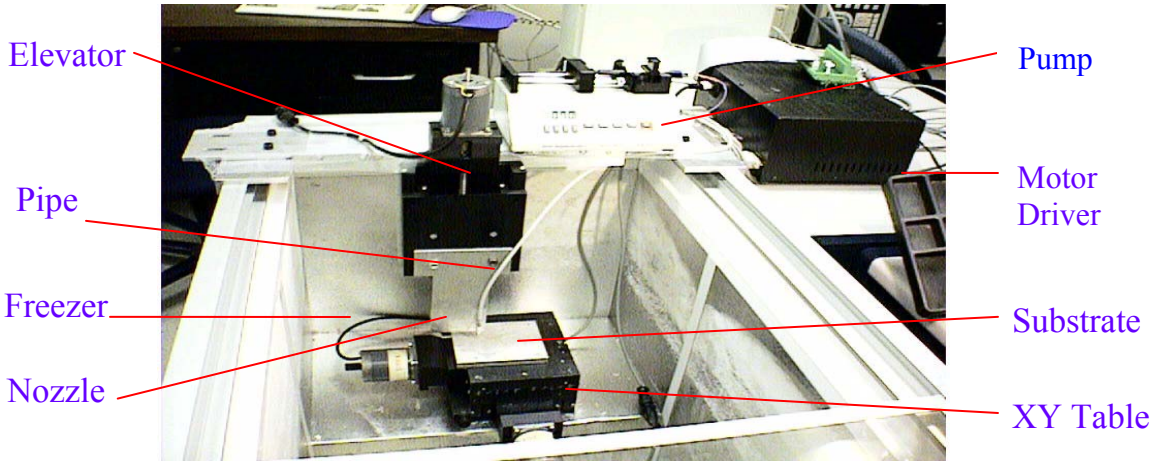

Figure 2.1. Rapid freeze prototyping (RFP) machine inside a deep freezer. Water is deposited on the liquid nitrogen chilled substrate, which is moved by the XY table.

Can molding involves pouring slurry around a pattern contained in a rigid structure (i.e., a can). After the slurry hardens, the pattern is melted out and metal is cast into the remaining void. Jose's [2005] research applied can molding and casting to threaded test articles and dental fixtures for dimensional analysis using ice patterns. He maintained a constant freezer temperature of -16°C. Water based colloidal silica binder systems could not be used to prevent ice pattern melting, so an ethyl silicate binder was chosen. Alumino-silicate flours and a triethanolamine catalyst were used to create investment casting molds. Particle size was 0.075 mm for the alumino-silicate flour, which was dried at 100°C for one hour before use. Ten weight percent ethyl silicate binder was diluted by 50% with ethanol to improve moldability. Jose found 46% solids loading was optimal for can molds. Jose [2005] used Grey Matter, a commercial alumino-silicate flour with small inorganic glass fibers premixed to increase strength and improve resistance to cracking during layered shell building.

Investment casters use mechanical mixing slurry tanks rotating at 15 to 18 rpm to prevent settling of the slurry. Past studies at Missouri University of Science and Technology noted that mixing slurry before dipping resulted in an increase in slurry temperatures of up to 10°C due to particle friction. This increase promoted pattern loss due to melting. A slurry tank was designed and built to fit inside a freezer, allowing the slurry to maintain proper suspension (i.e., preventing settling) and temperature (-15°C).

The initial design of the slurry tank system is shown in Figure 2.2. A five gallon bucket was rotated at 16 RPM. A cover reduced alcohol evaporation by increasing the local vapor pressure a K-type thermocouple monitored slurry temperature. An image of the system at work inside the freezer is also shown in Figure 2.2.

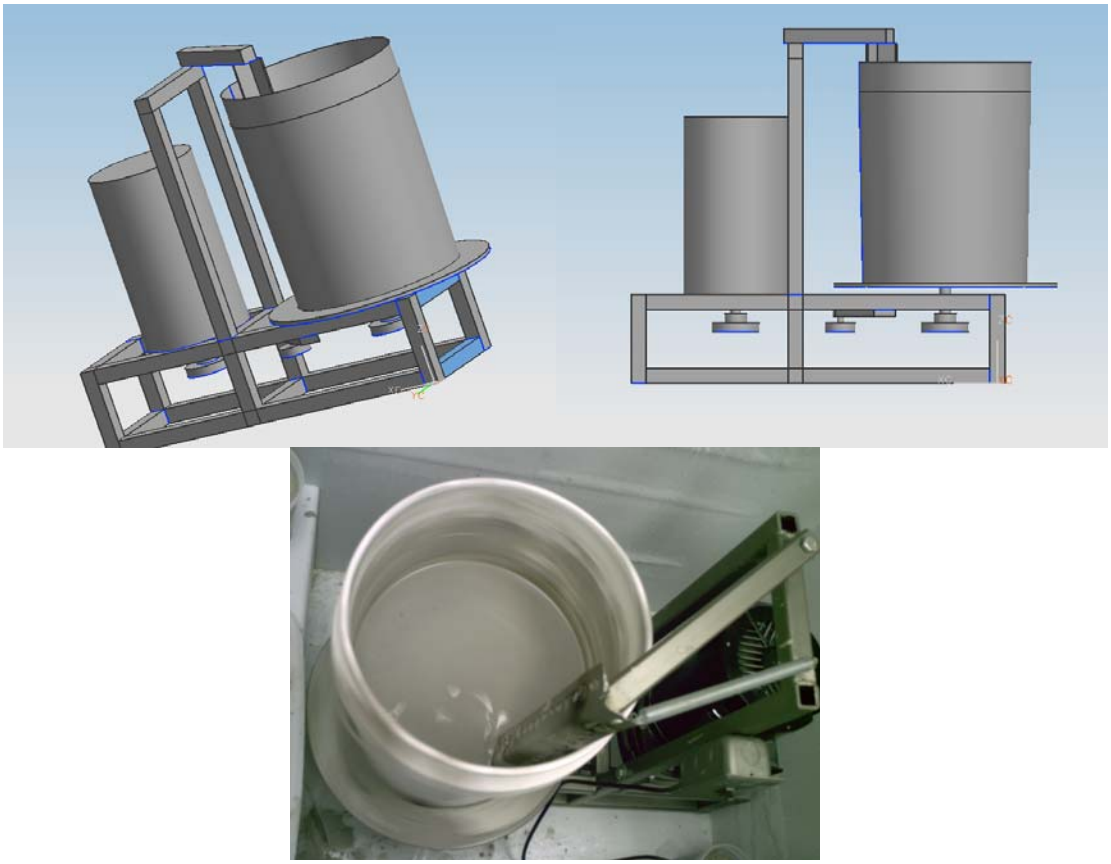

Figure 2.2. Schematic of slurry tank system. It is driven by an electric motor with built-in reducing gears (16rpm) rotating a five gallon bucket using a ½ inch drive belt.

A step plate pattern allowed for quantitative analysis of shell quality (surface finish) and pattern loss. The step plate's length and width allowed each step to be viewed as a semi-infinite plate. Step thickness varied between 0.38 mm (0.015 inches) and 6.35 mm (0.25 inches) thick, as shown in Figure 2.3.

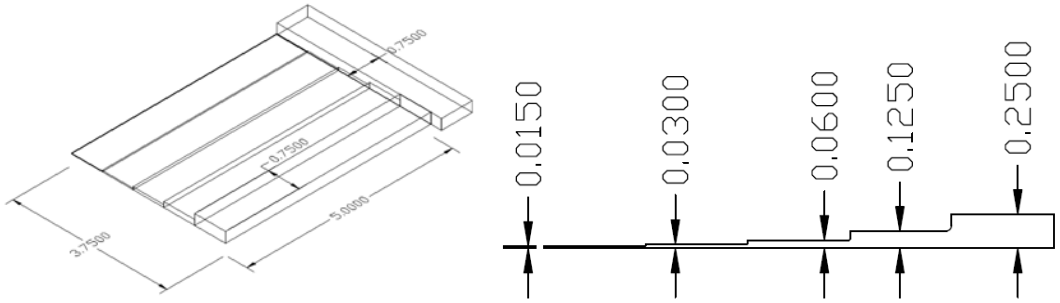

Figure 2.3. Step plate test article used for ice pattern, thin wall, investment casting trials (units are inches).

The shell was built in seven layers (Figure 2.4). The first layer (primary coat) determined the casting's surface finish and quality. The second and third layers (detail layers) build part detail. The fourth, fifth, and sixth layers (backup layers) produced the shell's strength. The final layer (a seal coat) was not stuccoed, and serves to bind the previous layer of stucco.

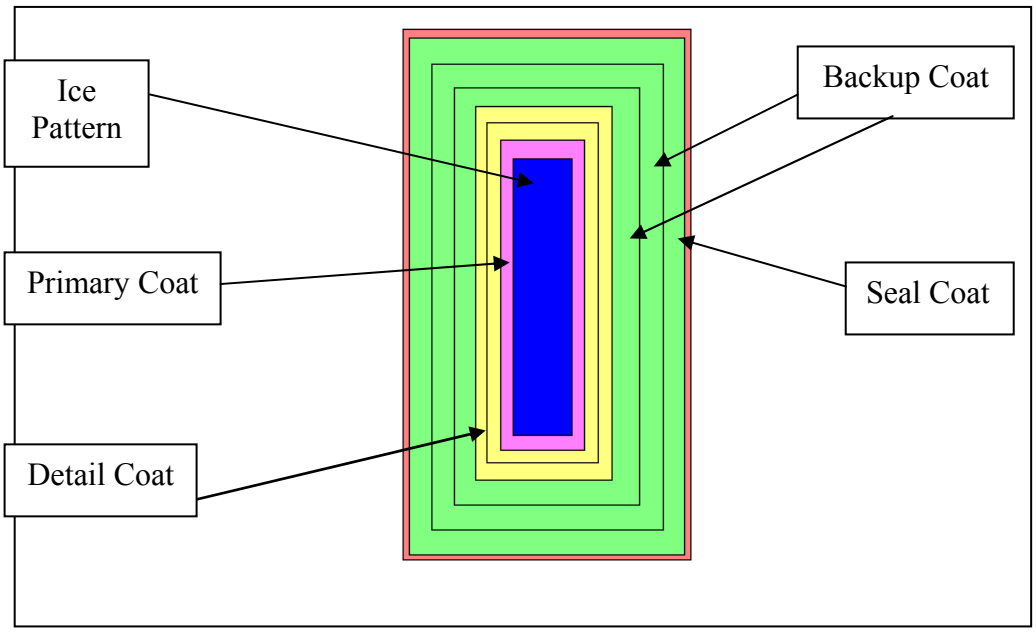

Figure 2.4. Diagram of shell coats: The primary coat determines surface finish, detail coats build pattern detail, backup coats provide strength, and the seal coat holds the last backup layer's stucco in place.

3. EXPERIMENTAL PROCEDURE

The interaction between pattern melt off (water) during the shell building process dilutes the primary coat, reducing the silica chain length and weakens the primary coat. Delaying catalyst application allows the ethanol carrier to evaporate, resulting in less dilution. Industry best practices delay catalyst application by 0.75 to 1.5 hours at room temperature for wax patterns; allowing ethanol to evaporate.

3.1. PATTERN LOSS

The goal of the pattern loss test was to determine if tridecane would reduce the interaction between the pattern and the slurry, thus reducing pattern loss. Twelve ice step-plates were produced for this test. Six of the plates received a double coating of tridecane; applied by dipping. The other six received no tridecane coating.

The primary coat consisted of 6900 mL of 10 wt.% ethyl silicate and 17 kilograms of a 50/50 mixture of alumino-silicate and fused silica flour. Remaining layers included 10% fiber to reinforce the fused silica flour. Primary coats did not contain fibers due to their potentially detrimental effect on surface quality. Step plate patterns were dipped in slurry, stuccoed with alumino-silicate sand, sprayed with catalyst (a 50/50 mixture of triethanolamine and ethanol), and cured for six hours. Stuccoing sand varied according to coat. Primary coat stucco was alumino-silicate 0-15 percent in sieve 150, 70-86 percent USS sieve 100, and 5-10 percent in sieve 50. Detail stucco was alumino-silicate of 9-22 percent sieve 100, 30-44 percent sieve 70, and 30-48 percent sieve 50. Backup stucco was alumino-silicate 27-37 percent sieve 40, 32-47 percent sieve 30, and 15-25 percent sieve 20. The seal coat was not stuccoed.

Images were taken of ice patterns prior to and after shell building and dewatering. Image analysis software was used to determine the initial thickness of the ice pattern steps and the final thickness of the shell cavity. Images were converted to grayscale for thresholding and adjusted so only the ice pattern (before) or shell cavity (after) was visible. Height measurements taken in 50 pixel increments were used to determine pattern loss as a function of initial thickness.

3.2. DELAYED CATALYST APPLICATION

A second test determined how long to delay catalyst application to maximize shell strength. Twelve four-point bend test bars were produced for each of three conditions. After stuccoing, catalyst was applied to shells with delays of zero, two, and four hours for each condition respectively and cured for a minimum of six hours. The primary coat slurry consisted of 17 kilograms of 200 mesh fused silica and 6900 ml of 20 wt% pre-hydrolyzed ethyl silicate. The remaining layers included fused silica flour, which contained ten percent fiber by weight. Slurry temperature was maintained at -13°C during shell building. Stuccoing was performed as described in section 3.1. The test bars were strengthened at 800°C for two hours. Test dimensions were approximately 3.8 inches (96.5 mm) long by 0.7 inches (18.5 mm) wide. Samples were tested using a Simpson Universal Sand Testing Machine and a four-point bend testing fixture. Load-at-failure was recorded in Newtons. Four-point bend strength was determined using Equation 1 [Baratta, 1982]:

$$S = \frac{3PL}{4bd^2} \tag{1}$$

where P = force, L = distance between supports, d = sample thickness, and b = sample width. This equation holds true only if the wedge stress is negligible between the support points and the loading points. This was achieved by minimizing the distance between the loading and support points in relation to sample thickness (typically a ratio of 1.2 to 1.4) and the almost negligible deflection of the bar before failure.

4. RESULTS

4.1. PATTERN LOSS

Three ice patterns (eight, nine, and twelve), which had not received a tridecane coating, broke during shelling. Samples one through six (tridecane coated) and samples seven, ten, and eleven (uncoated) survived shell building and dewatering. Figure 4.1 compares ice pattern starting thicknesses and resulting cavity thicknesses; Figure 4.2 illustrates the percentage loss for each step. Step one was the thickest step; thickness decreased for steps two and three. Step three was unquantifiable in samples four and five due to taper. The average coated step thickness of the ice was 7.56mm for step one, 4.87mm for step two, and 2.83mm for step three. Resulting cavity thickness was 7.00mm for step one, 4.08mm for step two, and 2.56mm for step three. A net loss of seven, sixteen, and five percent was found for each step respectively.

The average uncoated step thickness was 6.80mm for step one, 4.27mm for step two, and 1.83mm for step three. Cavity thickness for uncoated plates was 6.85mm for step one, 4.13mm for step two, and 2.43mm for step three. This resulted in a three percent net gain for step one, a three percent net loss for step two, and a 43% gain in thickness for step three. Careful examination of the mold cavities showed the

delamination of the primary coat in the third step of the uncoated plates, accounting for their increased size over the original pattern as shown in figure 4.3.

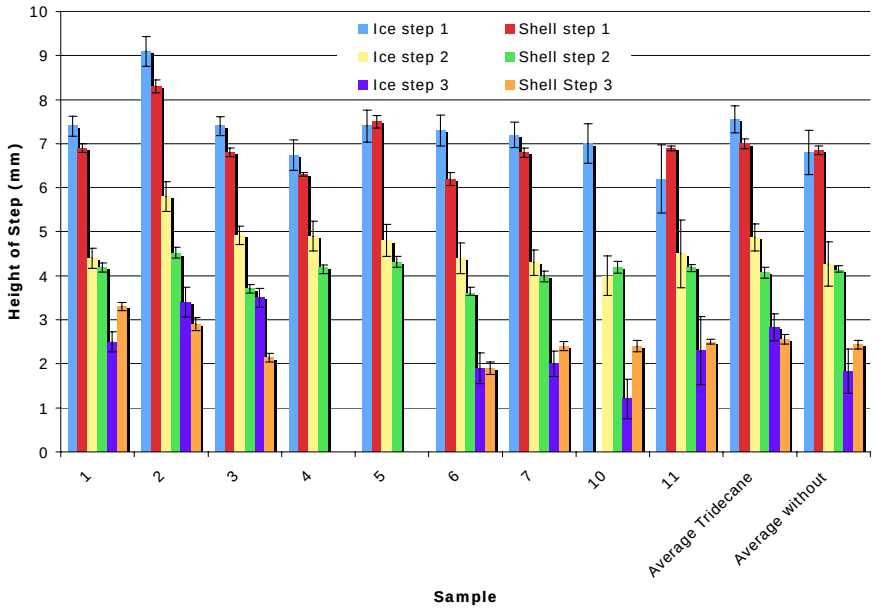

Figure 4.1. Ice pattern loss and resulting shell cavity thicknesses. Samples one through six were tridecane coated, samples seven, ten, and eleven were not coated. Delamination of the primary coat caused cavities to show a net increase in thickness.

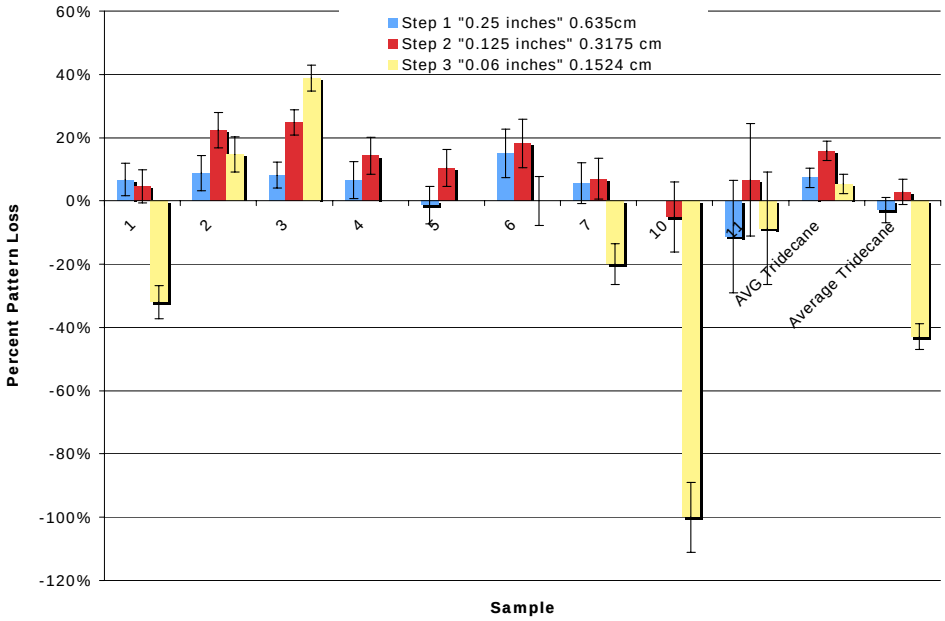

Figure 4.2. Percentage loss based on step thickness. Samples one through six (tridecane coated) experienced minimal loss of thickness compared to non-coated step plates.

Figure 4.3. Investment shell exhibiting primary coat delamination.

A sample of a tridecane coated pattern shell and a non-coated pattern shell were examined. Figure 4.4 shows complete primary coat loss in sections thinner than 1.52 mm (0.06 inches) for both conditions. The thickest two steps of the tridecane coated patterns retained the entire primary coat.

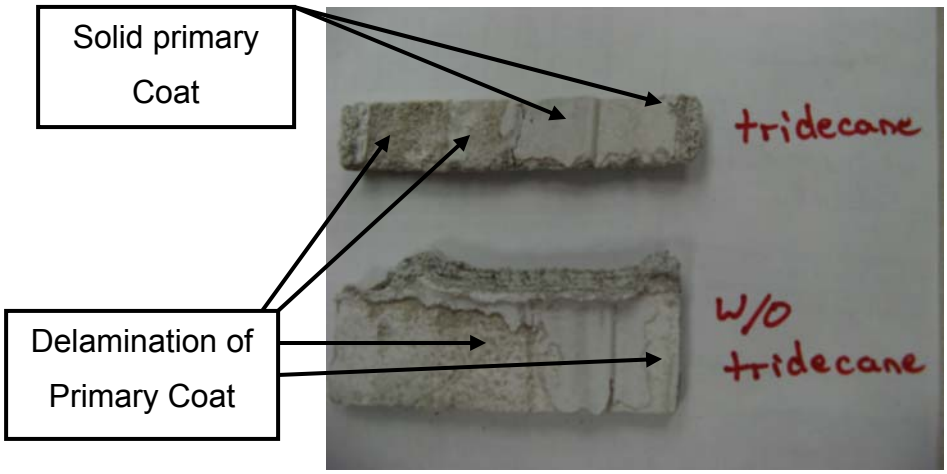

Figure 4.4. Step plate shells with and without tridecane coating. Tridecane coating increased retention of the primary coat. Step plate thickness increases from left to right.

4.2. DELAYED CATALYST APPLICATION

Initially, twelve four-point bend test bars were produced for each delay time. Several samples broke during sample preparation. Since the ice patterns were not coated with tridecane, this was presumably caused by the interaction of ethanol and ice. Any samples that broke during preparation or outside test fixtures inner supports were considered invalid. Table 4.1 contains the results for zero, two, and four hour delayed catalyst application times. Each column lists bar number and calculated strength (N/cm^2). There is an 88% probability that delaying catalyst application for four hours produced stronger shells (16.4 N/cm^2) compared to zero and two hours (11.7 and 14.5 N/cm^2 respectively).

Table 4.1. Four-point bend test results for delayed catalyst application. A four hour delay resulted in the highest average strength (16.4 N/cm^2).

	Sample Number and Strength (N/cm^2)									
Time Delay	One	Two	Three	Four	Five	Six	Seven	Eight	**Average**	**STDEV**
0 - Hours	10.1	18.2	9.8	10.9	11.4	9.9			**11.7**	**3.2**
2 - Hours	18.3	10.0	22.3	11.1	10.6				**14.5**	**5.5**
4 - Hours	12.3	10.9	9.8	28.0	10.9	15.7	20.3	23.5	**16.4**	**6.8**

5. DISCUSSION

5.1. PATTERN LOSS

Tridecane was not effective in preventing ice pattern loss for thicknesses of 1.52 mm (0.06 inches) and smaller. Thicker steps lost an average of seven percent of their starting thickness. Tridecane resulted in improved primary coat retention for the two thickest steps. Greater thermal mass increased the resistance to melting; presumably, thicker sections require greater heat input to cause melting and were, therefore, less affected by time outside the freezer during shell building. Increasing ice thickness required increased heat input to induce melting. Ice at -15°C and 0.40 mm thick was calculated to begin melting after 31 seconds at room temperature (25°C), whereas ice at -15°C and 6.35 mm thick will not begin melting for 360 seconds. Increasing the time delay before melting occurs would reduce pattern loss. The likelihood of water interacting with the primary coat would also be reduced, thereby increasing the primary coat strength.

5.2. DELAYED CATALYST APPLICATION

By delaying catalyst application for four hours after stuccoing, shell strength was increased from 11.7 N/cm^2 to 16.4 N/cm^2. Providing time for ethanol to evaporate before catalyst application resulted in higher silica chain lengths and increased strength.

6. CONCLUSION

Shells built on ice patterns suitable for counter gravity casting of metal-matrix aluminum composites can be produced using:

- tridecane interface agent coating
- 20 wt% ethyl silicate binder
- 20 wt% fiber-containing fused silica flour added after the primary coat
- Delay catalyst application by four hours
- -10°C environment.

Tridecane is an effective interface agent that produced stronger surface coats, particularly when combined with greater pattern thermal mass, which delays melting for a longer period of time. A -10°C or lower environment increased shell strength and improved surface finish. Tridecane resulted in reproducible minimization of ice pattern loss in ice 3.175mm (0.125 inches) thick.

7. FUTURE WORK

Future work should be conducted inside a freezer because ice pattern melting reduces pattern accuracy and shell strength. Additional methods of tridecane application should be explored. Further, emphasis should be placed on using RFP shells to produce actual castings. Finally, the pattern loss versus starting thickness experiment should be duplicated on rapid prototyped parts.

8. REFERENCES

Baratta, F. “Requirements for Flexure Testing of Brittle Materials.” AMMRC TR 82-20, Army Materials and Mechanics Research Center, Watertown, MA, 1982.

Jose, H. “Investment Casting Using Ice Patterns: Solid Mold and Shell Mold Methods” University of Missouri-Rolla: Thesis, 2005.

Yodice, A. “Freeze cast process ready for licensing”, INCAST: International Magazine of the Investment Casting Institute, 11(12), 19-21, 1998.

Yodice, A. “Freeze cast process”, US patent 5,072,770,1991.

Yodice, A. “Freeze process cuts casting costs”, Advanced Materials and Processes, 155 (4), 35-36, 1999.

III. Oxidation During Solidification of 15.5 PH Marine Propellers

Edward A. Druschitz

Missouri University of Science and Technology, Rolla, Missouri

Keywords: Investment Casting, Oxidation Formation, Shell Strengthening

1. ABSTRACT

Oxidation along the leading edge of cast Fe-15Cr-4.5Ni-3Cu (15-5 PH) stainless steel marine propellers requires costly non-value added finishing. The addition of an extra seal coat of slurry after autoclaving and a slower cooling rate can reduce this oxidation from 1.7 to 1.4mm^2mm^{-1} of oxidation per millimeter of blade length. This work showed that a seal coat applied after autoclaving re-saturated the shell filling in surface micro-cracking with slurry, delaying cracking and allowing the casting to cool adequately before exposure to an oxidizing atmosphere.

2. INTRODUCTION

The goal of this investigation was to reduce the amount and severity of oxidation along the leading edge of cast Fe-15Cr-4.5Ni-3Cu stainless steel (15-5 PH) marine propellers (Figure 2.1.) (Unless otherwise noted all chemistries are in weight percent).

Figure 2.1. Oxidation along the leading edge of a cast marine propeller.

According to Sosman [1927], the principal crystalline phases of silica are quartz, tridymite, crystobalite, and fused silica. When fused silica shells are heated above 1470°C (2678°F) they undergo devitrification to form a high temperature phase,

crystobalite. Sosman [1927] states that crystobalite undergoes a displacive transformation when cooled to temperatures of 200-275°C (392-522°F) at atmospheric pressure. Shells are formulated to develop fine cracking structure during cooling, resulting in easy removal. Transformation to crystobalite is controlled by mineralizer and time at temperature; typically sodium aids this transformation.

Lehman et al. [1995] notes that fiber additions date back to adobe, a dried clay reinforced with straw, to increase strength and toughness. A more modern example is concrete reinforced with steel rebar. Previous work conducted by Richards and Mascreen [2002] found fibers increased the strength of 4-point bend samples by causing crack deflection, wherein crack planes tilt and twist around surrounding grains and fibers.

According to Richardson [2006], brittle cracks propagate in low fracture toughness materials and result in high flaw sensitivity (low flaw tolerance). More recent work in fracture toughness, discussed by Richardson [2006], found dispersion of reinforcement materials of a higher elastic modulus will aid the material in carrying loads without fracturing.

According to Richardson [2006], cracking in a polycrystalline material can be broken down into three stages: 1) Stress induced energy is stored within the material, 2) crack nucleation occurs at the critical load on the largest flaw, and 3) stored energy drives crack propagation. Failure can be avoided by stress delocalization, accomplished by fiber reinforcement. Richardson [2006] suggests that the elastic modulus of fibers be two times that of the matrix. Short or “chopped” fibers of random orientation have gained wide acceptance within the ceramic industry and are utilized in investment casting foundries in such products as Grey Matter (fused silica flour containing small inorganic

fibers) [Nalco, 2004]. Typically, a fiber length-to-diameter ratio of 8:1 is the minimum necessary to allow proper modulus transfer from matrix to fiber. Randomly arranged chopped fibers can cause crack deflection and crack bridging, resulting in increased fracture toughness [Richardson, 2006].

Crack deflection depends on particle (i.e., grain or fiber) shape. Spherical particles increase toughness two-fold, whereas a disk can result in three-fold gains in toughness. Rods result in four-fold toughness improvements [Richardson, 2006]. Volume percentage of reinforcement particles is also important, as shown in Figure 2.2. which indicates that maximum effectiveness is achieved at 0.5 volume fraction regardless of shape [Richardson, 2006]. Brittle fiber achieved increased toughness via pull-outs, the expending of matrix energy resulting in reduced available crack propagation energy [Richardson, 2006].

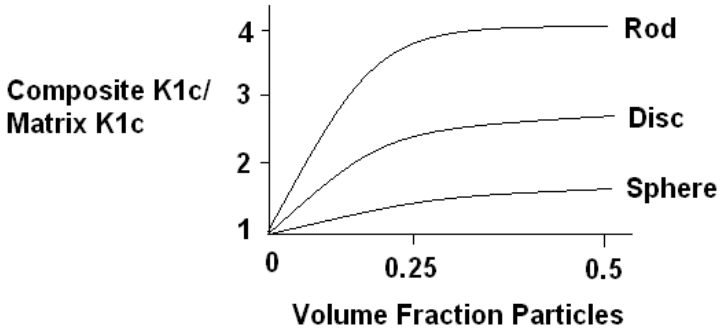

Figure 2.2 Effect of particle shape and volume fraction on fracture toughness [Richardson, 2006].

Ceramic shell building in most investment casting foundries follows similar procedural steps [AFS, 1993]. Patterns and gating are assembled and dipped into colloidal silica slurry and stuccoed with coarse refractory particles (typically fused silica).

Stucco is applied via “rain fall” sanders or by dipping into a fluidized bed [AFS, 1993]. Shell building typically consists of seven layers (Figure 2.3) [AFS, 1993]. The first layer (primary coat) determines the casting’s surface finish and quality. The second and third layers (detail layers) build part detail. The fourth, fifth, and sixth layers (backup layers) produce the shell’s strength. The final layer (a seal coat) is not stuccoed; it binds the previous layer of stucco.

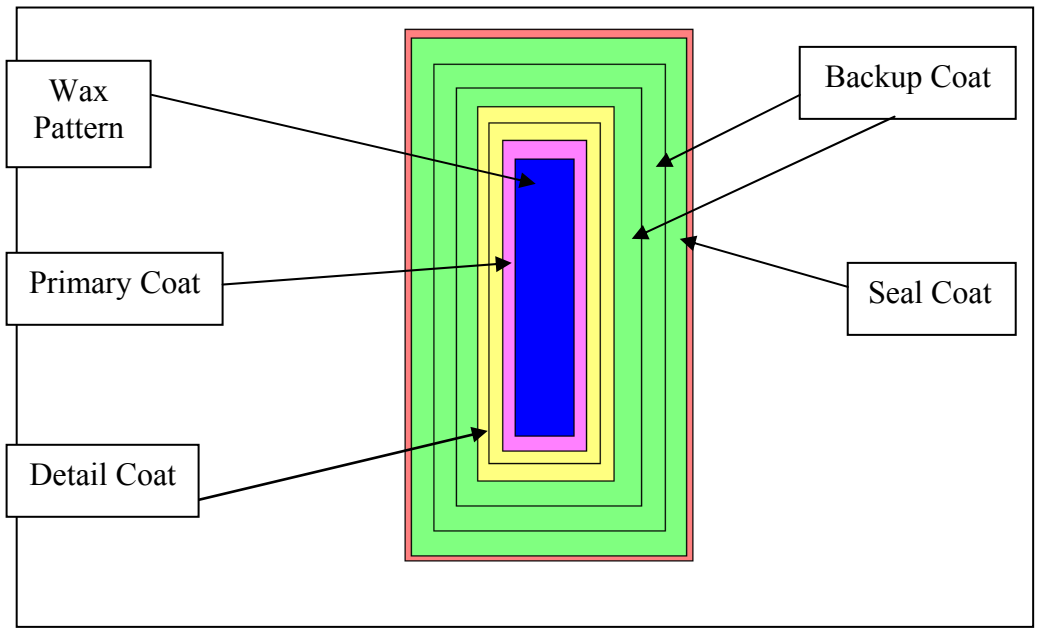

Figure 2.3. Diagram of shell coats, the primary coat determines surface finish, detail coats build pattern detail, backup coats provide strength, and the seal coat holds the last backup layer’s stucco in place.

Shells are dried for 24 hours before autoclaving to remove pattern wax. Autoclaves use high temperature, high pressure steam at eight atmospheres and 170°C (338°F) to melt wax patterns. Shells are then fired at 871-1093°C (1600-2000°F) to increase strength and remove residual organics before pouring in batches of three [AFS, 1993]. Shells are removed from firing three at a time, placed on a refractory brick lined cooling cart, and poured before placing the next batch. This process is repeated until all

shells have been cast. Post pouring, castings are cooled on the same cart on which they were poured. During cooling, the fused silica shell undergoes a displacive transformation resulting in cracking, allowing for easy removal of the shell from the thin metal casting.

Oxidation severity depends on composition, temperature, air flow, and exposure time [Lankford et al., 1985]. Blades on the outside of cart are surrounded by cooler air. Blades inside the cart cool slower, next to another blade of similar temperature (Figure 2.4). Slower cooling delays crystobalite inversion cracking, reducing exposure of the casting to air. Faster cooling causes the ceramic shells to crack sooner.

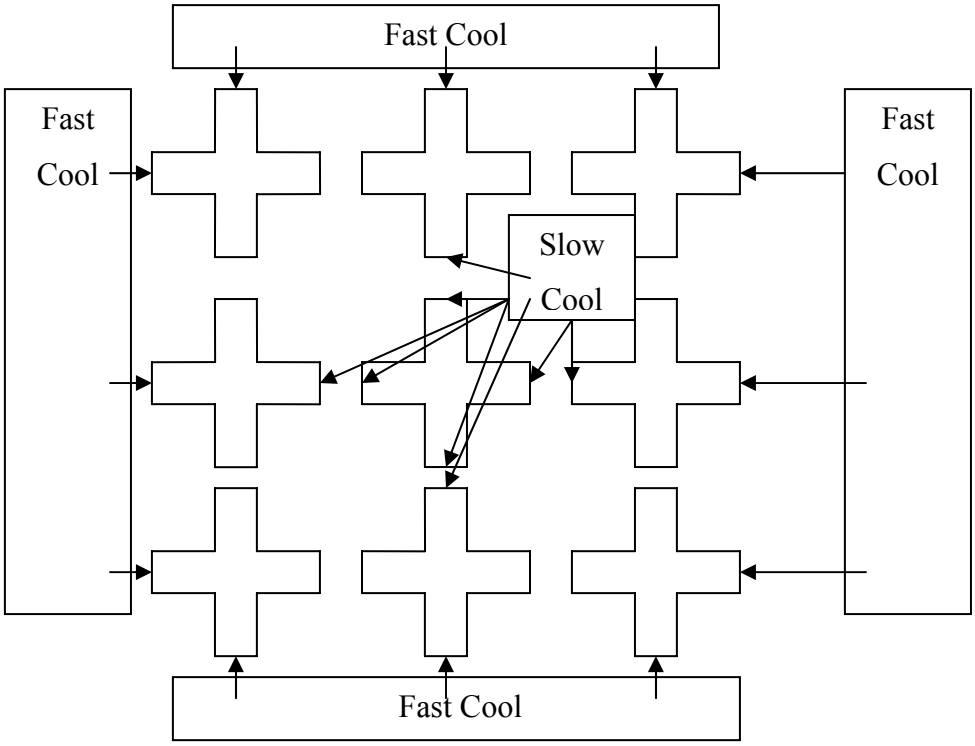

Figure 2.4. Illustration of cooling rate based on position. The inside propeller blades are surrounded by hot castings and will therefore cool slower.

Thermal images were taken and analyzed of castings poured at 1632°C (2970°F), which cracked at 428-460°C (802-860°F), as indicated in Figure 2.5 by red spots.

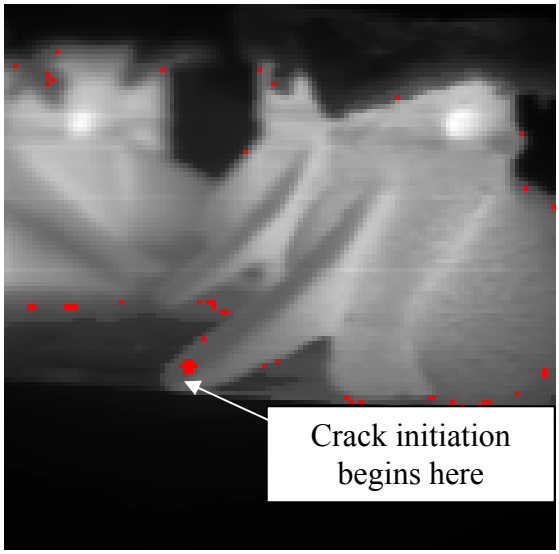

Figure 2.5. Thermal image of solidifying casting; areas in red indicate a temperature of 428°C (802°F).

EDS imaging showed that oxidation formed during solidification and cooling of cast 15-5 PH marine propellers was principally chromium oxide Cr_2O_3 (light areas) and silicon oxide SiO_2 (dark areas), as shown in Figure 2.6. The images were taken at taken at 20kV and a working distance of 19mm.

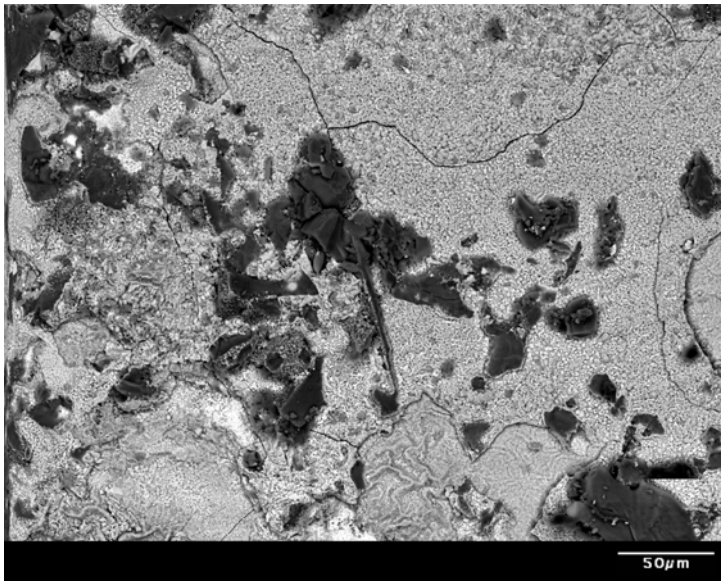

Figure 2.6. EDS image of leading edge oxidation of cast 15-5PH Stainless.

3. EXPERIMENTAL PROCEDURE

3.1. SHELL STRENGTHENING

Post autoclave seal coatings were tested as a method of delaying cracking onset during solidification. Six conditions were examined for this study, including baseline production, which received no seal coating. A seal coat of non-fiber-modified slurry and four fiber-modified slurry seal coats. De-waxed four blade propeller shells were utilized for these tests. An individual sample was defined as a single propeller blade. Two propellers (eight blades) were tested for each of the following conditions:

1. Baseline -- standard production (no modifications)
2. Extra seal coat of slurry (no fibers)
3. Extra seal coat with 0.3 wt% fibers
4. Extra seal coat with 0.8 wt% fibers
5. Extra seal coat with 1.1 wt% fibers
6. Extra seal coat with 1.5 wt% fibers

Images of each blade were taken with a high resolution digital camera after shake-out. Quantitative image analysis of oxidation was conducted using image analysis software. The leading edge length and oxidation area were determined (see Figures 3.1 and 3.2). These measurements permitted quantitative comparison of oxidation between blades by normalizing the data resulting in oxidation area per blade length ($mm^2/mm \pm$ one standard deviation).

Figure 3.1. Oxidation on leading edge of propeller blade.

Figure 3.2. Image analysis representation of oxidation on leading edge of propeller blade.

3.2. COOLING RATE EFFECTS

Eight autoclaved shells were given an extra seal coat and twenty-four hours to dry before burnout and pouring. These molds were placed in the middle row of the cooling cart (slow cooling). Eight production (non-modified) shells were also cooled on the middle of the cooling cart and thirty blades were cooled along the outside of the cooling cart as a control group. Quantitative image analysis was conducted in an identical manner to that of section 3.1.

4. RESULTS

4.1. SHELL STRENGTHENING

Table 4.1 contains the results of the shell strengthening test. Standard production shells resulted in 3.0 ± 0.6 mm^2/mm of oxidation per unit blade length on the leading edge of the propeller castings. An extra seal coat reduced oxidation per unit length to 2.6 ± 0.9mm^2mm^{-1} and 1.1 wt% fiber addition reduced oxidation to 2.6 ± 0.8mm^2mm^{-1}.

Table 4.1. Oxidation per unit length of blade (mm^2mm^{-1}).

	Oxidation per unit of Blade Length											
	Propeller 1				Propeller 2							
	Blade 1	Blade 2	Blade 3	Blade 4	Blade 5	Blade 6	Blade 7	Blade 8	Average	STDEV	Min	Max
Production	1.99	2.75	3.92	3.89	3.11	2.58	2.96	3.03	3.03	0.64	1.99	3.92
Extra Coat	1.63	3.01	3.73	1.36	1.83	3.25	2.98	2.96	2.60	0.86	1.36	3.73
0.3 wt%	1.97	3.81	5.03	5.26	5.41	2.52	3.55	4.39	3.99	1.27	1.97	5.41
0.8 wt%	3.51	2.94	1.73	7.27	3.28	1.85	1.83	4.30	3.34	1.84	1.73	7.27
1.1 wt%	3.24	2.85	3.65	1.98	2.20	1.26	2.08	3.14	2.55	0.80	1.26	3.65
1.5 wt%	2.30	1.92	2.97	3.01	2.49	3.22	3.71	3.37	2.87	0.59	1.92	3.71

Based on Chauvenet's criterion, a statistical means of assessing data outliers, one data point was removed from the 0.8 wt% fiber data set, reducing oxidation from 3.3 ± 1.8mm^2mm^{-1} to 2.8 ± 1.0mm^2mm^{-1}.

4.2. COOLING RATE EFFECTS

The average oxidation for production castings on the outside of the cooling cart is $1.7 \pm 0.7 mm^2 mm^{-1}$ compared to $1.5 \pm 0.5 mm^2 mm^{-1}$ for inside cooling. As shown in Table 4.2, propellers that received a seal coat and cooled slower had the least oxidation at $1.4 \pm 0.5 mm^2 mm^{-1}$ ($0.3\ mm^2 mm^{-1}$ less oxidation per mm of blade length when compared to outside cooled production castings). Cooling rate was never measured specifically. Oxidation per unit blade length was $0.2 mm^2 mm^{-1}$ lower for production molds cooled slowly inside rather than outside cooling.

Table 4.2. Oxidation ($mm^2 mm^{-1}$) as a function of position

	Test Condition		
mm2/mm of oxidation	Outside	Inside	Inside +Seal
Average	1.7	1.5	1.4
STDV	0.7	0.5	0.5
Minimum	0.5	0.8	0.4
Maximum	2.9	2.6	2.6
Sample Size	32	40	32

5. DISCUSSION

5.1. SHELL STRENGTHENING

Because a non-fiber reinforced seal coat reduced oxidation to $2.6 mm^2 mm^{-1}$ per unit blade length compared to 2.6-3.9 $mm^2 mm^{-1}$ for fiber additions it did not appear that fibers aided in strengthening the shells. There is a 72 percent probability that an extra seal coat reduced the oxidation versus standard production based on recorded data. Also, the 1.1 percent fiber addition showed a 78 percent probability of improvement compared to production shells. It appears as though a seal coat applied after autoclaving re-saturated the shell, filling in surface micro-cracking with slurry and adding thickness.

The additional seal coat increased the shells' overall load-bearing capacity which likely delayed cracking and allowed the casting to cool adequately before exposure to an oxidizing atmosphere.

5.2. COOLING RATE EFFECTS

There is a 70 percent probability that castings cooled more slowly inside have $0.2mm^2mm^{-1}$ less oxidation than quickly cooled outside castings. Presumably, the decreased oxidation is a result of allowing the casting to cool below 800°C before being exposed to oxygen. There is also a 95 percent probability that casting of shells receiving an extra seal coat and cooled slower experienced $0.3mm^2mm^{-1}$ less oxidation compared to production castings cooled faster.

6. CONCLUSION

By increasing the shell's load bearing capacity, toughness, the onset of cracking is delayed, and castings are able to cool enough to prevent severe oxidation (800°C) before cracking. These factors reduce the amount of oxidation per unit blade length by as much as $0.3mm^2mm^{-1}$.

7. FUTURE WORK

A cooling cart surrounded by refractory or encased by insulating fiber boards, should slow cooling sufficiently. Inert atmosphere during cooling may also reduce oxide formation. Modeling could determine optimal rates of cooling. Cooling rate and oxygen content of the air surrounding the castings should also be measured.

8. REFERENCES

American Foundrymen's Society. Handbook on the Investment Casting Process. Des Plaines, Illinois: American Foundrymen's Society, 1993.

Lankford, W.T., Jr., Samways, N.L., Craven, R.F., McGannon, H.E., editors, "The Making, Shaping, and Treating of Steel", 10th edition, Association of Iron and Steel Engineers, Pittsburgh, PA, 2985.

Lehman, R. L., El-Rahaiby, S. K., Wachtman, J. B. Jr., "Handbook on Continuous Fiber-Reinforced Ceramic Matrix Composites." Ceramics Infromation Analysis Center, West Lafayette, IN, 1995.

Nalco Company, "Grey Matter", Naperville, IL, 2003.

Richards, V. L., Mascreen, S., "Thermal Expansion of Investment Casting Pattern Wax", AFS Transactions, 2003.

Richardson, D. Modern Ceramic Engineering, Taylor and Francis Group, Boca Raton, FL, 2006.

Sosman, R. B., "The Phases of Silica", New Brunswick, Rutgers University Press, 1965.

APPENDIX

Modeling of Heat Transfer through Investment Casting Shells: Method of Determining Shell Thermal Conductivity

Edward A. Druschitz
Simon Lekakh
Dr. Von Richards

1. ABSTRACT

This work demonstrates a simple and inexpensive method for measuring thermal conductivity of investment casting shells. Reducing shell cracking during the autoclave-dewaxing cycle is a goal of all investment casting foundries. However, before cracking can be reduced, the factors that contribute to crack initiation and propagation must be established. Shell cracking can lead to many surface defects, including heavy oxidation resulting in pitting. These discontinuities can be removed only by non value-added manual labor, increasing the overall cost of a casting. Although extensive work on modeling the autoclave dewaxing process has been conducted at a number of universities and by numerous research facilities, most of this work has either relied on assumptions regarding thermal conductivity of the shells or measured shell thermal conductivity using expensive and bulky equipment plus, including a production autoclave. Such measurements require production downtime.

2. INTRODUCTION

The investment casting process is similar to that used in the ancient world: Modern investment casting foundries use robots to dip wax pattern trees, ceramic

materials (such as fused silica) are applied in layers to create shells, and steam autoclaves (boilerclaves) are used to remove the wax from the shells. The basic investment casting procedure is shown in Figure 1.

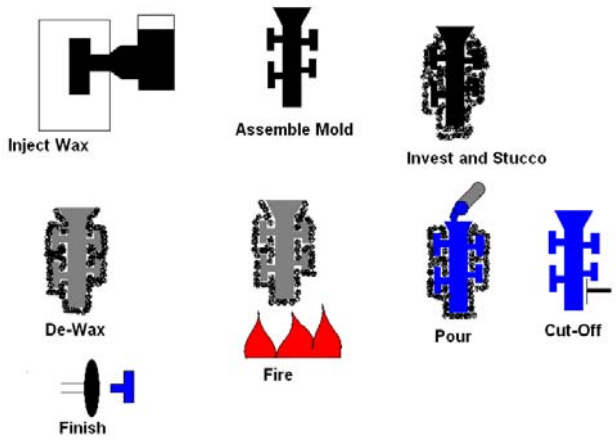

Figure A.1. Basic investment casting procedure.

The single greatest factor determining the quality of an investment casting is the shell into which the metal is poured. No step in the investment casting process affects shell quality more than autoclaving. Snow [2] suggests that 90% of all shell cracks originate in the autoclave; fins, dimensional problems, shell debris, and leakers are all results of these cracks. The autoclave is a pressure vessel that uses high temperature steam to aid in the extraction of the wax from the shell. However, this relatively simple machine is a modern day "black box" for the simple reason that quantifying what goes on inside an autoclave is difficult, requiring expensive equipment that can withstand pressures up to 10 bar and temperatures as high as 180°C (Gebelin[3]). During the autoclave dewaxing cycle, high temperature steam penetrates the porous ceramic shell (changing the thermal conductivity of the shell), transferring heat to the wax, and thus

causing the wax to melt and run out of the shell cavity (Gebelin J-C[4]). Work conducted by Connolly[5] suggests that the specific heat of a ceramic shell could be calculated using the rule of mixtures. This equation, which treats each shell component (stucco and slurry) as an individual element, is labeled below as Equation 1.

Equation 1. (Connolly[5])

$$Cp_{Shell} = F_1 Cp_1 + F_2 Cp_2 + F_3 Cp_3 ...$$

where:

Cp_{Shell} = Specific heat capacity of the investment shell as a whole

F_1 = Fractional mass of material 1

Cp_1 = Specific heat capacity of material 1

Connolly[5] used a differential scanning calorimeter (DSC) and Equation 2 to determine the specific heat capacity of each shell component, i.e., the primary coat slurry, primary coat stucco, and so on

Equation 2. (Connolly[5])

$$\Delta\Theta_{SR} = \Theta_S - \Theta_R = Cp_s \frac{\delta T_S}{\delta t} - Cp_R \frac{\delta T_R}{\delta t} = (Cp_s - Cp_R)\beta$$

where:

$\Delta\Theta_{SR}$ = Differential heat flow rate

Θ_S = Heat flow from sample

Θ_R = Heat flow from reference

Cp_S = Sample specific heat capacity

δT_S = Temperature change in sample

Cp_R = Reference specific heat capacity

δT_R = Temperature change in reference

δt = Change in time

β = Average heating rate

Connaly[5] applied the specific heat capacity values generated for the individual components using the DSC to Equation 1 to calculate the overall specific heat capacity for the shell. He then compared those values to a measured C_p of the whole shell. The results were very similar, thus proving that the Rule of Mixtures can be used to calculate the C_p value of an investment shell. However, this procedure did not consider the effects of water infiltration or condensation in the shell.

Although Connolly's[5] work explained the speed with which the investment shell heated up in an autoclave, it failed to address the heat transfer through the shell to the underlying wax. Jones[6] corrected this deficiency by building a shell around a copper plate of known size and heating it in both wet and dry conditions. For the wet tests, the shelled plate was submerged in cold and hot water, and the temperature change of the copper plate over time was recorded. Following this procedure, the shell was removed and the average shell thickness was determined. Rearranging Equation 3 to find the

shell's thermal conductivity, Jones[6] was able to determine the thermal conductivity of the shell based on the heat flow through it.

Equation 3. (Jones [6])

$$K_s = \left(\frac{M_{Cu} C_{p,Cu} l_S}{A_S} \right) \left(\frac{\left(\frac{\delta T_{Cu}}{\delta t} \right)}{\left(T_{Cu} - T_{fl} \right)} \right)$$

Analysis of the data showed that the thermal conductivity of the shell was approximately 0.4 – 0.55 W/m^{o}K in the dry condition and 0.9 – 1.1 W/m^{o}K in the wet condition. This result demonstrated that the thermal conductivity doubled when water filled the porous ceramic shell (Jones [6]). This dramatic increase in thermal conductivity is favorable since it would create a smaller thermal gradient across the shell, thus decreasing the depth of the wax melt front and reducing the amount of bulk wax expansion that might cause the shell to crack.

Sabau[7] expanded on the work of Heames and Geiger (1978), Huang et al. (1989) and Hendricks and Engelhardt (1993) by further developing the theory of packed beds as a useful model to explain the thermal conductivity of sintered (fired) fused silica shells. Sabau's[7] research examined two methods to measure the thermal conductivity of the shells, the hot-wire method (ASTM C1113) and laser-flash (ASTM C714). After preliminary experimentation, Sabau found that the Laser-Flash method was too sensitive to the shell's thickness and yielded inconsistent results; therefore, he settled on a form of the hot-wire test to determine shell thermal conductivity. This work demonstrated that the hot wire method can determine shell thermal conductivity and emissivity, which

could aid in the modeling of shell thermal properties during cooling. A semi-empirical correlation for thermal conductivity indicated that the radiative component of the thermal conductivity can, be expressed as Equation 4 (Sabau[7]).

Equation 4. (Sabau[7])

$$K_r(T) = 4EBd_pT^3$$

where:

K_r = Radiative component of thermal conductivity

E = Factor of order correlated to radiation properties

B = Stefan-Boltzman constant

d_p = Particle size

T = Absolute temperature (K)

Sabau used this equation as a basis to determine emissivity, which he would later use to determine the heat transfer coefficient (HTC) from the shell to the ambient air. Until research progressed to this point, thermal conductivity of the shells was largely based on lab experiments that had yet to be verified by actual instrumented autoclave trials. Using a specially built high temperature test cell, Kruse[8] was able to invest a copper plate and actually record the temperature increase during a typical autoclave cycle. This data was used to calculate, for the first time, the thermal conductivity of the shell during the autoclave process using:

Equation 5. (Kruse [8])

$$\frac{MC_p\Delta T}{t} = \left(k\frac{A}{X}\right)\left(T_S - T_{Cu}\right)$$

Using this equation, Kruse [8] calculated the thermal conductivity and pressure of a foundry's shells to be 0.5 W/m^{o}K dry and 1.4 W/m^{o}K wet. For dry shells, this trial yielded the same results as published by Jones[6] but it showed that high temperature pressurized steam resulted in a higher thermal conductivity. According to Kruse[8], during the autoclave cycle, the air is compressed 87.5 percent, and the condensed steam is pulled into the underlying shell by capillary action. During Kruse's[8] tests, the thermal conductivity increased by 2.0 – 2.5 times depending on shell structure and composition. Presumably, this increase occurs because the conductivity of the shell changes with both saturation and temperature, indicating that existing models of two-phase structures did not adequately represent the shell's thermal conductivity. Kruse[8] proposed a revised Maxwell model in which the thermal conductivity of the continuous phase (ceramic and polymer) was also affected by the moisture content. The underlying physics used to justify this approach was that the polymer and colloidal silica at the contact points of the refractory grains absorb water and thus change both the cross-sectional area and the properties of the contact points. This assumption would be important later when Sabau[7] adopted the hot wire method to create an inexpensive and non-intrusive test to determine the thermal conductivity of shells.

Various mechanisms of heat transfer may be involved during shell bulging in the investment casting process. The shell, which is a highly porous structure, could transfer

heat by: 1) thermal conductivity through a skeleton of solid fused silica particles, 2) by air conductivity in closed pores, with 3) additional air convection in open interconnected pores and, finally, 4) radiation during firing and pouring at high temperature. In addition, wax removal in the autoclave is assisted by water vapor, which could also dramatically change the rate of heat transfer as a result of the high thermal conductivity of water and heat of condensation liberation. It is difficult to develop a theory that takes into account all these possibilities. The experimental methods typically used to measure heat transfer have been based on steady state measurement techniques. These measurements require that samples be placed between a heat source and a heat sink, and the temperature gradient reflects the value of the coefficient of thermal conductivity. Unfortunately, steady state methods do not accurately reflect real non-steady-state industrial processes, such as shell dewaxing in an autoclave. Non-steady-state measurement techniques are more attractive because they can provide data representing combined variables, including temperature, thermal conductivity, heat capacity, and thermal diffusivity.

Thermal diffusivity is a material's ability to adjust its temperature to the surroundings quickly; it is expressed in Equation 6. Heat diffusivity is the ability of the shell to absorb heat (heat diffusivity = $k\rho C_p$) (Poirier[10]). Equation 7 shows the heat flux into a mold. The rate at which latent heat is evolved is shown in equation 8 (Poirier[10]). During the solidification of a casting, the amount of solidified material depends on the characteristics of the metal's (T_m, T_o, p and H_f) and the heat diffusivity of the mold materials (k, p and C_p) (Poirier[10]). During the autoclave dewaxing process, liquefaction occurs. The same information needed to determine solidification times is also required to

model the autoclave process; however, the parameters for melting wax are used in place of those for solidifying metal.

Equation 6: (Poirier [10])

$$\alpha = \frac{k}{\rho C_p}$$

Equation 7: (Poirier [10])

$$q \int_{X=0} = \frac{\sqrt{k\rho C_p}}{\sqrt{\pi t}} * (T_m - T_0)$$

Equation 8: (Poirier [10])

$$q \int_{X=0} = \rho H_f \left(\frac{\delta M}{\delta t} \right)$$

Equation 9: (Poirier [10])

$$M = \frac{2}{\sqrt{\pi}} * \left(\frac{(T_M - T_0}{\rho H_f} \right) \sqrt{k\rho C_P} \sqrt{t}$$

Two standard methods are used for non-steady-state heat transfer measurements. The first, called the hot wire method, creates a known value of heat energy inside the media using a micro heater. A K-type thermocouple is used to determine the temperature

curve, and the thermal conductivity (k) can be determined from the temperature versus time curve. The thermal conductivity of the sample can be derived as follows:

Equation 10: (Carlsaw [11])

$$\Delta T = \left(\frac{Q}{4\pi k_s} \right) * \left(\ln(t) + A \right)$$

Equation 11: (Yamasue [12])

$$A = \ln\left(\frac{4\alpha_S}{r^2 C_e} \right) + \frac{k_s}{2k_w} + \ldots$$

where r is the radius of the wire, Ce is Euler's constant, and α is the thermal duffusivity of the sample. Typically, the thermal conductivity of the sample is the slope of the linear relationship between ΔT and ln(t), calculated as:

Equation 12: (Yamasue [12])

$$k_s = \left(\frac{Q}{4\pi} \right) \left(\frac{\delta \Delta T}{\delta \ln(t)} \right)^{-1}$$

The second method is a transient technique, the laser flash method. This method measures heat diffusivity and requires additional measurements or assumptions in terms of the value of specific heat capacity.

3. EXPERIMENTAL PROCEDURE

The present work has developed a novel method for dynamic measurement of thermal processes in unsteady thin shells and bulk sand media. This method is based on the generation of a stable and known value for an energy impulse created by passing direct current through a wire microheater, combined with temperature measurements inside the media near the heat source. The micro impulse of heat has minimal influence on existing thermal processes and properties of the sand media. The relaxation time after the current is turned off is short and therefore permits the reproduction of cyclic measurements of the thermal properties in rapidly changing conditions. Also, the device simultaneously measures the absolute temperature of the media.

The microheater was made from 0.38 mm Alomega wire and was approximately 15 mm long. The microheater was welded to thicker wire (0.8 mm) of the same material to concentrate the heat impulse on the measured space. A type K thermocouple (0.38 mm wire for fast response) was used for temperature measurement. Alumina tube (05 mm in diameter) with four holes was used for the shell of the device. A high resolution, 24-bit data acquisition system and programmable power supply were connected to a PC. Programming was done with LabView 8 software, which supplied precise voltage/current/time parameters. A schematic of the device is shown in Figure 2.

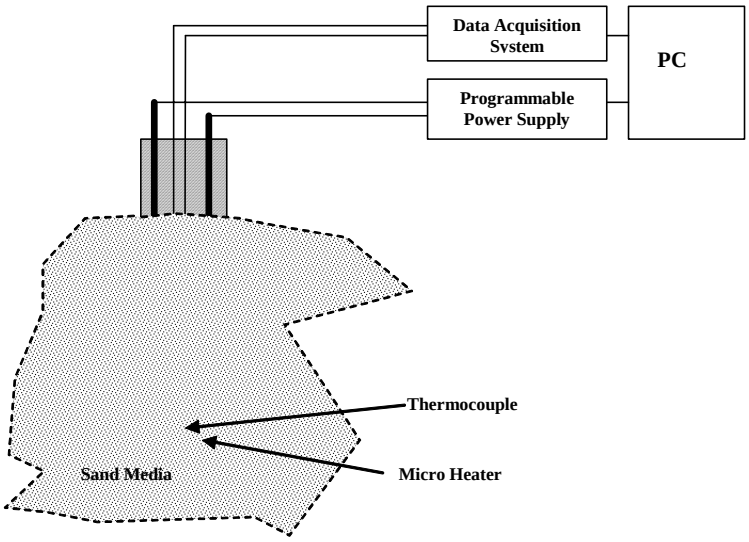

Figure A.2. Method of unsteady thermal conductivity measurements.

The new method was first tested using bulk dry sand. Temperature impulses at various levels of impulse energy are shown in Figure 3. The measured amplitude of the temperature impulse was increased with increasing electrical current and heating time. The amplitude of temperature impulse had minimal variations in sequential measurements when the same electrical impulse was applied. Full temperature relaxation time increased from 1 minute for a 1A/3 sec heat impulse to 5 minutes for a 3A/60 sec heat impulse. Relaxation time refers to the minimum possible time between sequential measurements. The necessary test cycle can be designed with a programmable power supply.

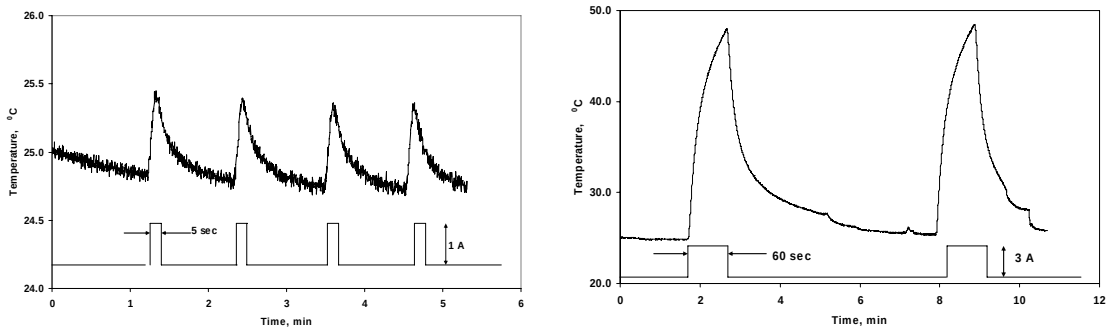

a) b)

Figure A.3. Measured temperature in bulk dry sand for a) 1A and 5 sec impulse and b) 3A and 60 sec impulse.

The sensitivity of this new method was tested using sand with varying moisture contents. The last composition was chosen to evaluate the potential influence of media electro-conductivity on measurement results. In addition, mixtures of dry sand and mineral oil were tested to determine the potential influence of water on short circuiting and heat generation. The applied electrical impulses were 2A for 120 seconds. The initial measurement data is provided in Figure 4a, and the influence of the moisture and oil additives on the amplitude of the temperature change is shown in Figure 4b. In both cases, this method indicated that the temperature increase in the sand media with more thermally conductive liquid (water or oil) was far less than without. The measurement technique was not affected by the electrical conductivity of the liquid.

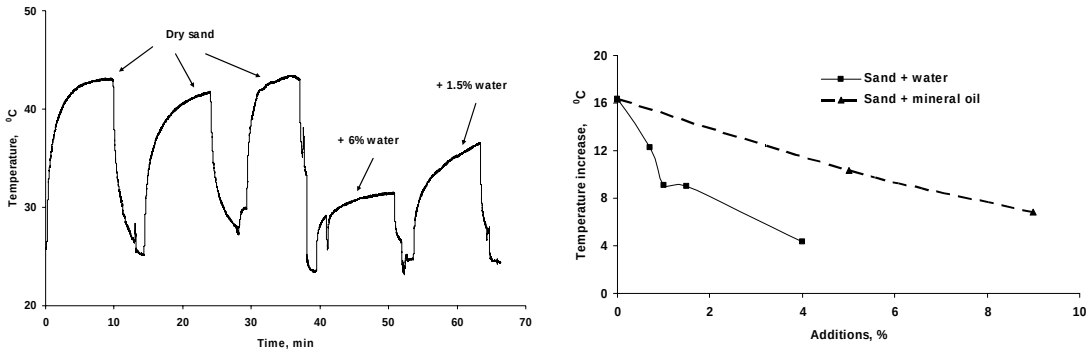

a) b)

Figure A.4. Influence of moisture and mineral oil additions to dry sand on the amplitude of the temperature increase.

4. COMPUTER MODELING

Fluent software was used to model unsteady heat transfer in 3D media with an internal energy source (wire). Fluent is a finite element modeling package; for this work, a 3-node edge, quadrilateral face, and hexahedral volume were used. The semicircle picture in Figure 5a represents the internal energy source, which was operated in the open position (2A) and closed position (0A) using a constant resistivity. The thermocouple was located between the two legs of the semi-circle. The boundary and initial conditions used in this preliminary modeling ignored the thermal resistance between the materials at their boundaries because the thermal conductivity of the shell material was already very low. The principle equation used by Fluent is shown in equation 13 (Fluent [13]). Temperature dependent values of heat capacity Cp are shown in equation 14; they were applied to the wire heater and shell media without additional thermal resistance (Fluent [13]).

Equation 13: (Fluent [13])

$$\frac{\delta}{\delta t}\rho h = \frac{\delta}{\delta x_i}\left(k\frac{\delta T}{\delta x_i}\right) + q$$

where: ρ is density, h is enthalpy (which equals $\int_{T_{ref}}^{T} C_p dT$), k is thermal conductivity, T is temperature, and t is time.

Equation 14: (Fluent [13])

$$k_{Wire}\left(\frac{\delta T}{\delta x}\right)_{Wire} = k_{Media}\left(\frac{\delta T}{\delta x}\right)_{Media}$$

The model used published thermal properties of bulk dry sand, and the results were compared to experimentally measured temperature increases at 2A, as shown in Figure 5.

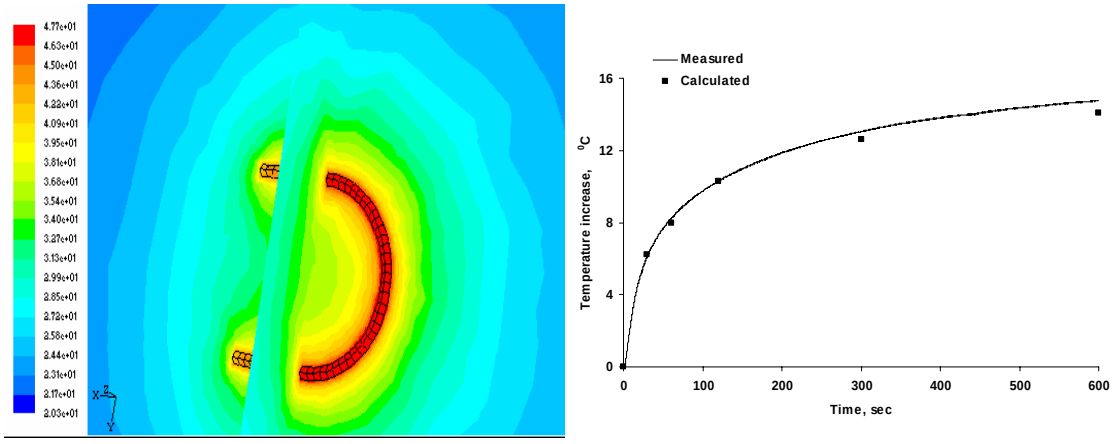

a) b)

Figure A.5. Computed temperature field (a) and comparison of experimentally measured temperature increase with calculated data for dry bulk sand (b).

The calculated temperature increase was similar in media with different known values of thermal conductivity as shown in Figure 6.

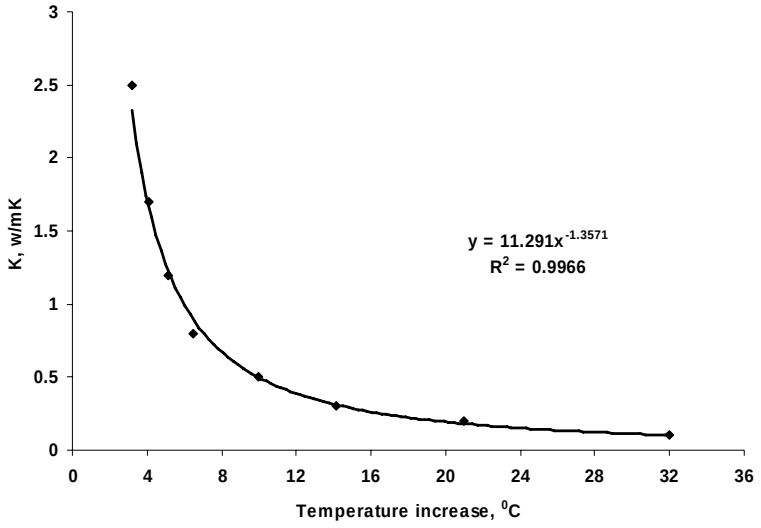

Figure A.6. Calculated temperature increase and K of materials

5. EXPERIMENTAL RESULTS

Three shell probes were created, and investment shells were built on them. Sample 1 is a production built shell representing the entire shell building process (primary coat and secondary coats) at a participating foundry. Samples 2 and 3 are from different foundries; sample 2 received only primary coats, and sample 3 received only backing coats. Pictures of these samples are shown in Figure 7.

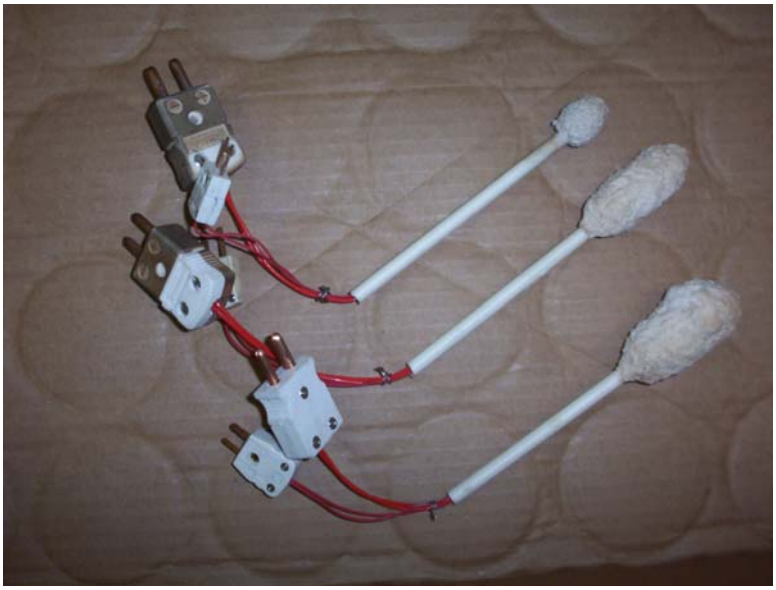

Figure A.7. Completed thermal conductivity probes.

Three shells were tested using different conditions (specified in Table 1). The shells were initially submerged in dry sand and tested. Tests were then conducted in steam by isolating the samples in a Kaowool box and using a continuously working steamer at 60-90°C and normal atmospheric pressure. The samples were also tested while submerged in water for 20 minutes. The temperature increase (°C) was measured and the thermal conductivity (k) calculated, results are shown in Table 1.

Table A.1. Results of initial round of shell thermal conductivity testing.

Test conditions	Sample 1 - primary & backing		Sample 2 – primary only		Sample 3 – backing only	
	T, °C increase	K, W/m^{o}K	T, °C increase	K, W/m^{o}K	T, °C increase	K, W/m^{o}K
Initial shell	17.85	0.23	9.29	0.55	10.33	0.48
In steam	9.8	0.52	6	1.0	5.96	1.01
In water	5.9	1.02	4.77	1.36	5.8	1.05

6. RESULTS AND DISCUSSION

Past work conducted by Brandon Kruse[8] at the Missouri University of Science and Technology to develop a similar shell conductivity test required a large insulating test chamber to shield the data acquisition system from the intense heat and pressure created inside the autoclave. During his trials, Kruse coated a copper block with a production ceramic shell similar to samples 2 and 3 described above. Sample 2 demonstrates the thermal conductivity of the primary coat, and sample 3 demonstrates that of the backing coat. The present work evaluated each of the shell layers separately to determine if grain size had an effect on the shell's thermal conductivity. Two observations are note worthy: first, when dry, samples 2 and 3 showed similar thermal conductivity (0.55 and 0.48 W/m°K). Second, the thermal conductivity of the primary sand (sample 2) was 1.36 W/m°K when submerged in water. Prior work conducted by Kruse[8] showed similar results in a production shell (with both a primary coat and backing coats). During his trial runs, the dry shell had a thermal conductivity of approximately

0.64 W/m°K, and at saturation in the autoclave the thermal conductivity was approximately 1.56 W/m°K using the Maxwell model (Kruse [8]). The thermal conductivity of the finer primary sand was 0.31 W/m°K higher than the backing sand when saturated, likely because the smaller grain size led to high interconnectivity. Thus heat was transferred through the backing faster by conduction. Also, the density of the finer prime coat stucco was higher than that of the coarser backing stucco, and pore size was greater in the backing stucco. Further, the difference between the saturated results of the hot wire test and Kruse's[8] tests may be the pressure at which the autoclave operates. At eight atmospheres of pressure, air in the autoclave would be compressed 87.5% and the steam would be pulled through the shell by a capillary effect (Kruse [8]).

7. CONCLUSIONS AND RECOMENDATIONS

The hotwire method permits accurate measurement of the thermal conductivity of an investment shell without requiring a production autoclave in which to run tests. Also, the small probes can easily be shipped to the foundry where the samples can be invested in the materials of interest to the lab. Thus, there is no need for a lab technician to travel to each location. Knowing the thermal conductivity of an investment casting shell will permit more precise modeling of what happens inside the autoclave and thus aid in the understanding and reduction of shell cracking.

Future work for this project will include the creation of numerous sample probes. These probes will be sent to participating foundries to be shelled, and then mailed back for testing. These tests will aid in both the development of a more accurate autoclave model and clarify how various parameters, including shell slurry, stucco, and grain size,

affect the thermal conductivity of shells. In addition, this information will aid in the further development of the autoclave model.

8. ACKNOWLEDGEMENTS

The authors would like to thank Mercury Marine Corporation and O'Fallon Casting for their support of this project, and the Mercury Marine Propeller Division for their time, patience, and dedication to this work.

This report is based upon work supported by the U.S. Department of Energy under Award No. De-FC36-04GO14230. Any findings, opinions, conclusions, or recommendations expressed here are those of the authors and do not necessarily reflect the views of the Department of Energy.

9. BIBLIOGRAPHY

1. American Foundrymen's Society, "Investment Casting Process", American Foundrymen's Society, 1993.

2. J. Snow, "What Happens During Autoclave Dewaxing," Proc. 46th Annual Technical Meeting of the Investment Casting Institute, 1998, paper 5.

3. Gebelin J-C, Jones S and Jolly M, "Modeling of the De-Waxing of Investment Cast Shells", computational Modelling of Materials, Minerals, and Metals Processing, TMS, 2001.

4. Gebelin J-C, Jolly M.R and Jones S. "Process Modelling Research for Investment Casting," Proc. 48th Annual Technical Metting of the Investment Casting Institute, 2000.

5. Connolly S, Jones S, Marquis P.M, Ford D.A. "Specific Heat of Investment Casting Shells" 10th World Conference on Investment Casting, Paper 8.

6. Jones S. Jolly M.R. Blackburn S. Gebelin J-C. Cendrowicz A. and Lewis K. "Effect of moisture upon mechanical properties of ceramic moulds during high pressure steam dewaxing," Materials Science and Technology, July 2003, Vol. 19.

7. Sabau A.S. and Viswanathan S, "Thermophysical Properties of Zircon and Fused Silica-Based Shells for Investment Casting," AFS Transactions, 2004.

8. Kruse B. and Richards V. "Thermal and Moisture Characterization During Autoclave Dewaxing in Investment Casting," SFSA T&O Conference Paper No. 5.5: 2005.

9. Holman J.P. "Experimental Methods for Engineers," McGraw-Hill. Hightstown, NJ. 1994.

10. Poirier D.R. and Geiger G.H. "Transport Phenomena in Materials Processing", TMS 1994.

11. Carlsaw H. S. and Jaeger J. C. "Conduction of Heat in Solids", Oxford at the Clarendon Press, 1947.

12. Yamasue E, Masharhiro S, Hiroyuki F and Kazuthiro N. "Nonstationary Hot Wire Method with Silica-Coated Probe for Measuring Thermal Conductivities of Molten Metals." Metallurgical and Materials Transactions A, Volume 30A, August 1999.

13. Fluent Incorporated. "Fluent 5 User's Guide." Fluent Incorporated, Volume 2, 1998.

VITA

Edward Alan Druschitz was born on June 8, 1983 in Michigan. He grew up in Rochester Hills, Michigan, before moving to Troy, Michigan. In the eighth grade, he moved to Lynchburg, Virginia where he lived until graduating from Jefferson Forest High School in 2001. He earned his Bachelors degree in Mechanical Engineering Technology from Central Washington University in 2005 before following his dream to study metallurgical engineering technology at Missouri University of Science and Technology (formerly University of Missouri-Rolla) where he earned his master's degree in 2009.